

Computationally Efficient Markov Chain Monte Carlo Methods for Hierarchical Bayesian Inverse Problems

D. Andrew Brown* Arvind K. Saibaba† Sarah Vallélian‡

July 13, 2022

Abstract

In Bayesian inverse problems, the posterior distribution can be used to quantify uncertainty about the reconstructed solution. In practice, approximating the posterior requires Markov chain Monte Carlo (MCMC) algorithms, but these can be computationally expensive. We present a computationally efficient MCMC sampling scheme for ill-posed Bayesian inverse problems. The forward map is assumed to be linear with additive Gaussian noise, and the goal is to reconstruct the solution as well as to estimate regularization parameters. We employ a Metropolis-Hastings-within-Gibbs (MHwG) sampler with a proposal distribution based on a low-rank approximation of the prior-preconditioned Hessian. We show the dependence of the acceptance rate on the number of eigenvalues retained and discuss conditions under which the acceptance rate is high. We demonstrate our proposed sampler through numerical experiments in electroencephalography and computerized tomography.

Keywords: computerized tomography, electroencephalography, low rank approximation, Metropolis-Hastings independence sampler, prior-preconditioned Hessian

1 Introduction

In engineering and applied mathematics, a common problem of interest is that of recovering quantities that cannot be directly observed, but only measured indirectly in the presence of measurement error. Such problems arise in many applications, including medical imaging [32], earth sciences [3], and particle physics [46], to name a few. The deterministic approach to inverse problems involves minimizing an objective function to obtain a single point estimate of the solution. Inverse problems admit also a Bayesian interpretation, facilitating the use of prior information and allowing full quantification of uncertainty about the solutions in the form of a posterior probability distribution. An overview of Bayesian approaches to inverse problems is available in [37, 44, 70]. A recent special issue of *Inverse Problems* also highlights the advances in the Bayesian approach and the broad impacts of its applicability [13].

In the Bayesian statistical framework, the possibly high-dimensional parameter of interest, \mathbf{x} , is modeled as random variable in addition to the observed data, \mathbf{b} . *A priori* uncertainty \mathbf{x} is quantified in the prior distribution, $\pi(\mathbf{x})$. Bayesian inference then proceeds by updating the information about the parameter given the observed data. The updated information is quantified in the posterior distribution, obtained via Bayes' rule, $\pi(\mathbf{x}|\mathbf{b}) = f(\mathbf{b}|\mathbf{x})\pi(\mathbf{x}) / \int f(\mathbf{b}|\mathbf{x})\pi(\mathbf{x})d\mathbf{x} \propto f(\mathbf{b}|\mathbf{x})\pi(\mathbf{x})$, where $f(\cdot|\mathbf{x})$ is the assumed data generating model determined by \mathbf{x} , also called the likelihood. Rather than providing a single solution to the inverse problem, the Bayesian approach provides a distribution

*Department of Mathematical Sciences, Clemson University, Clemson, SC 29634; ab7@clemson.edu;

†Department of Mathematics, North Carolina State University, Raleigh, NC 27695; asaibab@ncsu.edu;

‡Statistical and Applied Mathematical Sciences Institute, Research Triangle Park, NC 27709; svallelian@samsi.info;

of plausible solutions, thereby enabling uncertainty quantification. The posterior distribution makes available any desired estimator, along with measures of uncertainty about that estimator (e.g., the variance of the posterior). Formal decision rules then may be employed to obtain a Bayes estimator with respect to a particular loss function, the most common being 0-1 loss (classification) and squared error loss (estimation). The Bayes estimators with respect to these loss functions are the maximum a posteriori estimator (MAP; the posterior mode) and the posterior mean, respectively.

A popular deterministic approach to solving the inverse problem is Tikhonov regularization [73] in which the objective function to be minimized includes a regularization term to find the best solution subject to specified constraints; e.g., the minimum norm solution. This approach is closely related to the statistical notion of ridge regression [35]. From a Bayesian perspective, the objective function corresponds to a model in which both the likelihood and the prior about the estimand are assumed to be Gaussian. Placing prior distributions on the error precision and the prior precision parameters in the two Gaussian distributions gives the data freedom in determining plausible values of these parameters in the posterior, inducing a posterior distribution on the regularization term in the objective function. Sampling from the posterior distribution thus allows for simultaneous estimation of hyperparameters, as well as quantifying the reconstruction uncertainty.

Determination of regularization parameters has received considerable attention in the inverse problems community. Standard approaches for regularization parameter selection include the discrepancy principle [64], cross-validation [50], the L -curve approach [28, 31], and the unbiased predictive risk estimator [50]. A review of these approaches is provided in [30]. Another approach to estimating regularization parameters is to use χ^2 tests [42, 43]. Hybrid iterative methods, such as [39, 15, 16], use an iterative approach such as the Lanczos or Golub-Kahan bidiagonalization method to generate a basis for the Krylov subspace and search for optimal regularization parameters using one of the approaches mentioned above. In contrast to the iterative approaches that only focus on reconstructing point estimates, our proposed approach allows for simultaneously reconstructing parameters and estimating uncertainties.

A challenge of the fully Bayesian approach is that the posterior distribution will usually result in integrals that cannot be evaluated analytically. In this case, Monte Carlo approximations can be used to approximate the quantities of interest. Even Monte Carlo, however, requires samples from the posterior distribution, which are generally unavailable so that indirect sampling approaches are necessary. The most common set of techniques for accomplishing this is Markov chain Monte Carlo (MCMC) [21]. Several MCMC methods for sampling the resulting posterior distribution obtained from inverse problems have been proposed in the literature [7, 19, 9, 1, 10]. However, these methods can be computationally expensive on large-scale problems due to the need to factorize a large covariance matrix at each iteration. There are, however, instances in which the choice of the prior and the forward operator lead to a dramatic reduction in computational cost [8]. More generally, a wide variety of methodologies have been proposed in the Bayesian literature to address the computational problem presented by high-dimensional MCMC. Many such methods involve either projecting the data onto a lower-dimensional space and modeling in that space (e.g., [34], [33], [4]), carrying out sequential MCMC algorithms over successively refined resolutions (e.g., [75]), or posterior approximations such as variational Bayes ([51]).

This work addresses the computational burden incurred by a standard block Gibbs algorithm by exploiting the mathematical structure of the inverse problems, in particular the low-rank structure of the forward model. The computationally expensive part of a block Gibbs algorithm is drawing repeated samples from the high-dimensional Gaussian distribution of the estimand, conditional on the remaining parameters and the data. To approximate this step, we use a Metropolis-Hastings-within-Gibbs algorithm and sample from a proposal distribution based on a low-rank approximation to the prior-preconditioned Hessian, which is easy to construct and to sample from. We derive explicit formulas for the acceptance rate of our proposed approach and analyze its statistical properties, demonstrating its concentration near one as the spectrum of the prior-preconditioned Hessian decays. We provide a detailed description of the computational costs. Numerical experiments on challenging applications from neuroimaging confirm the theoretical properties of our proposed sampling approach

and demonstrate the computational benefits over standard approaches.

The rest of the paper is organized as follows. In Section 2, we formulate a general linear inverse problem in the hierarchical Bayesian framework. We outline the connection between the classical and statistical problem and discuss the choice of prior distributions. In Section 3, we briefly review Markov chain Monte Carlo, including Gibbs sampling and the Metropolis-Hastings algorithm. We highlight the computational bottleneck in standard block Gibbs sampling and, in Section 4, we propose an independence Metropolis-Hastings-within-Gibbs algorithm to reduce the computational burden without sacrificing the quality of the results. We demonstrate the performance of our algorithm on simulated examples in image deblurring, EEG, and CT reconstruction in Section 5. The paper concludes with a discussion in Section 6 and proofs of stated results in an Appendix.

2 The Bayesian Statistical Inverse Problem

Assume that the observed data are corrupted by additive noise so that the stochastic model for the forward problem is

$$\mathbf{b} = \mathbf{A}\mathbf{x} + \boldsymbol{\epsilon}, \quad (1)$$

where $\mathbf{A} \in \mathbb{R}^{m \times n}$ is the forward operator, or the parameter-to-observation map, $\boldsymbol{\epsilon}$ is the measurement error, and \mathbf{x} is the underlying quantity that we wish to reconstruct. We suppose that observational noise $\boldsymbol{\epsilon}$ is a Gaussian random variable with mean zero and covariance $\mu^{-1}\mathbf{I}$, independent of the unknown \mathbf{x} . In some applications, μ may be known *a priori*. Quite often, however, it is unknown and thus we assume that is the case here. Under this model, $\mathbf{b} \mid \mathbf{x}, \mu \sim \mathcal{N}(\mathbf{A}\mathbf{x}, \mu^{-1}\mathbf{I})$ so that the likelihood is

$$f(\mathbf{b} \mid \mathbf{x}, \mu) \propto \mu^{m/2} \exp\left(-\frac{\mu}{2}(\mathbf{b} - \mathbf{A}\mathbf{x})^\top(\mathbf{b} - \mathbf{A}\mathbf{x})\right), \quad \mathbf{b} \in \mathbb{R}^m. \quad (2)$$

The prior distribution for \mathbf{x} encodes the structure we expect or wish to enforce on \mathbf{x} before taking the forward model into account. An often reasonable prior for \mathbf{x} is Gaussian with mean zero and covariance $\sigma^{-1}\boldsymbol{\Gamma}_{\text{pr}} = \sigma^{-1}(\mathbf{L}^\top \mathbf{L})^{-1}$; i.e.,

$$\pi(\mathbf{x} \mid \sigma) \propto \sigma^{n/2} \exp\left(-\frac{\sigma}{2}\mathbf{x}^\top \boldsymbol{\Gamma}_{\text{pr}}^{-1} \mathbf{x}\right), \quad \mathbf{x} \in \mathbb{R}^n, \quad (3)$$

where the covariance matrix $\boldsymbol{\Gamma}_{\text{pr}}$ is assumed known up to the precision σ .

Different covariance matrices may be chosen depending on what structure one wishes to enforce on the estimand \mathbf{x} . In this work, we consider two different choices for the covariance matrix $\boldsymbol{\Gamma}_{\text{pr}}$. The first choice is a Gaussian process in which $(\boldsymbol{\Gamma}_{\text{pr}})_{ij} = \kappa(\mathbf{r}_i, \mathbf{r}_j)$, where $\kappa(\cdot, \cdot)$ is a covariance kernel and $\{\mathbf{r}_j\}_{j=1}^n$ is a set of spatial coordinates corresponding to spatial grid locations. Several choices of covariance kernel are possible, with the most common being in the Matérn family [55]. The second choice is motivated by Gaussian Markov random fields (GMRFs) [59]. In this approach, the precision matrix is expressed as the discretized representation of the differential operator $(\kappa^2 - \Delta)$. A link between Gaussian processes and GMRFs is reviewed in [40]. An advantage of the GMRF representation is that the precision matrix is sparse and thus computationally efficient to handle. In contrast, Gaussian processes more easily accommodate stationarity and generally allow for smoother fields. However, the covariance kernels have infinite support so that the resulting covariance matrices are dense. This is computationally challenging for large-scale applications. Fast Fourier Transform-based approaches on regular grids (e.g., [2]) and the \mathcal{H} -matrix approach on irregular grids (e.g., [61, 62]), though, can make the computational costs comparable to those associated with GMRFs.

We take the prior distributions of both the noise and prior precisions in (2) and (3) to be the conjugate Gamma distribution, $\mu \sim \Gamma(\alpha_\mu, \beta_\mu), \sigma \sim \Gamma(\alpha_\sigma, \beta_\sigma)$;

$$\begin{aligned} \pi(\mu) &\propto \mu^{\alpha_\mu - 1} \exp(-\beta_\mu \mu), \quad \alpha_\mu, \beta_\mu > 0 \\ \pi(\sigma) &\propto \sigma^{\alpha_\sigma - 1} \exp(-\beta_\sigma \sigma), \quad \alpha_\sigma, \beta_\sigma > 0, \end{aligned} \quad (4)$$

where the coefficients $\alpha_\mu, \beta_\mu, \alpha_\sigma$, and β_σ are fixed. It has been observed that the Gamma prior on σ can be inappropriate for situations in which \mathbf{x} is thought to be sparse, since it can artificially force the variance σ^{-1} away from zero [53]. Attractive alternatives for modeling the variance include Jeffreys' prior [71], the proper Jeffreys' prior [65], or the half-Cauchy prior [22], with the half-Cauchy often suggested as a suitable 'default' option. Our proposed approach simplifies sampling from the distribution of \mathbf{x} conditional on the variance components, though, and is the same regardless of the priors on σ or μ . We use the Gamma prior for convenience.

With μ and σ fixed, the conditional posterior of $\mathbf{x} \mid \mathbf{b}, \mu, \sigma$ is $\mathcal{N}(\mathbf{x}_{\text{cond}}, \mathbf{\Gamma}_{\text{cond}})$, where $\mathbf{\Gamma}_{\text{cond}} \equiv (\mu \mathbf{A}^\top \mathbf{A} + \sigma \mathbf{\Gamma}_{\text{pr}}^{-1})^{-1}$ and $\mathbf{x}_{\text{cond}} \equiv \mu \mathbf{\Gamma}_{\text{cond}} \mathbf{A}^\top \mathbf{b}$; i.e.,

$$\pi(\mathbf{x} \mid \mu, \sigma, \mathbf{b}) \propto \exp \left(-\frac{\mu}{2} \|\mathbf{Ax} - \mathbf{b}\|_2^2 - \frac{\sigma}{2} \|\mathbf{Lx}\|_2^2 \right).$$

The conditional posterior mode, $\hat{\mathbf{x}} = \arg \max_{\mathbf{x}} \pi(\mathbf{x} \mid \mu, \sigma, \mathbf{b})$, is obtained by minimizing $(\mu/2) \|\mathbf{Ax} - \mathbf{b}\|_2^2 + (\sigma/2) \|\mathbf{Lx}\|_2^2$ with respect to \mathbf{x} . This criterion is equivalent to generalized Tikhonov regularization in the deterministic linear inverse problem. While many commonly used point estimators have been related to the solution of the ill-posed inverse problem [18, 50, 74], we see here the particular connection between deterministic MAP estimation and that of finding the posterior mode of the conventional Bayesian Gaussian-Gaussian model with fixed variance components.

By assigning prior distributions to μ and σ (hence inducing a prior on $\lambda = \sigma/\mu$), the posterior distribution allows us to estimate plausible values of the regularization parameter determined by the data. Such values may be missed when deterministically estimating the regularization parameter through, e.g., cross-validation or L -curves [19]. However, with priors on the variance components, the full posterior distribution is no longer Gaussian and generally not available in closed form, necessitating the use of sampling methods to explore it.

3 MCMC Sampling Methods

3.1 Metropolis-Hastings

For some target distribution with density $h(\boldsymbol{\theta})$, the Metropolis-Hastings (MH) algorithm proceeds iteratively by generating at iteration t a draw, $\boldsymbol{\theta}_*$, from an easily available proposal distribution possibly conditioned on the current state, $\boldsymbol{\theta}_{(t-1)}$, and setting $\boldsymbol{\theta}_{(t)} = \boldsymbol{\theta}_*$ with probability

$$\alpha(\boldsymbol{\theta}_{(t-1)}, \boldsymbol{\theta}_*) = \min \left\{ \frac{h(\boldsymbol{\theta}_*) q(\boldsymbol{\theta}_{(t-1)} \mid \boldsymbol{\theta}_*)}{h(\boldsymbol{\theta}_{(t-1)}) q(\boldsymbol{\theta}_* \mid \boldsymbol{\theta}_{(t-1)})}, 1 \right\}, \quad (5)$$

where $q(\cdot \mid \boldsymbol{\theta}_{(t-1)})$ is the density of the proposal distribution. This algorithm produces a Markov chain $(\boldsymbol{\theta}_{(t)})$ with transition kernel

$$K(\boldsymbol{\theta}, \boldsymbol{\theta}_*) = \alpha(\boldsymbol{\theta}, \boldsymbol{\theta}_*) q(\boldsymbol{\theta}_* \mid \boldsymbol{\theta}) + \delta_{\boldsymbol{\theta}}(\boldsymbol{\theta}_*) \left(1 - \int \alpha(\boldsymbol{\theta}, \boldsymbol{\theta}') q(\boldsymbol{\theta}' \mid \boldsymbol{\theta}) d\boldsymbol{\theta}' \right),$$

where $\delta_{\boldsymbol{\theta}}(\cdot)$ is the point mass at $\boldsymbol{\theta}$. Provided that $\text{supp } q(\cdot \mid \boldsymbol{\theta}) = \text{supp } h(\cdot)$, this transition kernel satisfies detailed balance with respect to the target density $h(\cdot)$ and hence the distribution associated with h is the stationary distribution of the MH Markov chain [56]. If the Markov chain is aperiodic and irreducible with respect to h , then the distribution associated with h is the limiting distribution of this chain for any initial state. A sufficient condition for h -irreducibility is [57]

$$q(\boldsymbol{\theta}_* \mid \boldsymbol{\theta}) > 0 \quad \forall (\boldsymbol{\theta}_*, \boldsymbol{\theta}) \in \text{supp } h \times \text{supp } h.$$

The basic Metropolis-Hastings algorithm is given in Algorithm 1.

Provided the aforementioned conditions on the chain hold, the Metropolis-Hastings algorithm converges to the target distribution regardless of the initial distribution. However, as the target

distribution is only the limiting distribution of the chain, it may take several hundred or several thousand transitions of the chain before the realized states closely approximate draws from the target distribution. Thus, when implementing this algorithm, it is common to discard the first few hundred (or few thousand) iterations of the chain as a so-called “burn-in” or “warm-up” period before sampling from it [23].

A particularly important special case of the MH algorithm is Gibbs sampling [26]. The basic algorithm is to update the elements of $\boldsymbol{\theta} = (\theta_1, \dots, \theta_p)^\top$ one at a time through the collection of full conditional distributions with densities $g_j(\theta_j \mid \boldsymbol{\theta}_{-j})$, $j = 1, \dots, p$, where $\boldsymbol{\theta}_{-j} = (\theta_1, \dots, \theta_{j-1}, \theta_{j+1}, \dots, \theta_p)^\top$. The algorithm can be expressed as collection of p MH updates, where the j^{th} proposal density is $q_j(\boldsymbol{\theta}_* \mid \boldsymbol{\theta}) = g_j(\theta_{*,j} \mid \boldsymbol{\theta}_{-j})\delta_{\boldsymbol{\theta}_{-j}}(\boldsymbol{\theta}_{*,-j})$; hence each of the acceptance probabilities in (5) is equal to one [23, 57]. When a subset of the parameters is highly correlated in the target distribution, sampling one component at a time inside the Gibbs sampler causes the chain to move very slowly through the parameter space, leading to slow convergence. In this case it is usually more (statistically) efficient to update the correlated group of parameters all at once. This is called *block Gibbs sampling* [41]. Block Gibbs sampling is the same as ordinary Gibbs sampling where one or more of the elements $\boldsymbol{\theta}_j$ is multivariate.

Input: Target density $h(\boldsymbol{\theta})$, proposal density $q(\cdot \mid \boldsymbol{\theta})$, chain length N , burn-in period N_b .
Output: Approximate sample from the distribution with density h , $\{\boldsymbol{\theta}_{(t)}\}_{t=N_b+1}^N$.

```

1 Initialize  $\boldsymbol{\theta}_{(0)}$ .
2 for  $t = 1$  to  $N$  do
3   Draw  $\boldsymbol{\theta}_* \sim q(\boldsymbol{\theta}_* \mid \boldsymbol{\theta}_{(t-1)})$  and  $u \sim \mathcal{U}(0, 1)$ .
4   if  $u \leq \alpha(\boldsymbol{\theta}_{(t-1)}, \boldsymbol{\theta}_*)$  then Set  $\boldsymbol{\theta}_{(t)} = \boldsymbol{\theta}_*$ . else Set  $\boldsymbol{\theta}_{(t)} = \boldsymbol{\theta}_{(t-1)}$ .
5 end

```

Algorithm 1: The Metropolis-Hastings algorithm.

3.2 Independence Sampling

A type of MH sampling relevant to our proposed approach is the *independence sampler*. An independence MH sampler proposes states from a density that is independent of the current state of the chain, so that the proposal is $q(\boldsymbol{\theta}_* \mid \boldsymbol{\theta}_{(t-1)}) \equiv q(\boldsymbol{\theta}_*) = g(\boldsymbol{\theta}_*)$. In this case, the ratio in (5) can be written as

$$\frac{h(\boldsymbol{\theta}_*)g(\boldsymbol{\theta}_{(t-1)})}{h(\boldsymbol{\theta}_{(t-1)})g(\boldsymbol{\theta}_*)} \equiv \frac{w(\boldsymbol{\theta}_*)}{w(\boldsymbol{\theta}_{(t-1)})}, \quad (6)$$

where $w(\boldsymbol{\theta}) \propto h(\boldsymbol{\theta})/g(\boldsymbol{\theta})$. The MH independence sampler is very similar to the *accept-reject algorithm*. The accept-reject algorithm draws a candidate value X from an available generating distribution with density g such that $h(x) \leq Mg(x)$, for some $M \geq 1$, for all x , then accepts the draw with probability $h(X)/Mg(X)$, resulting in a draw from the target distribution.

For both independence sampling and accept-reject methods, it is desirable for g to match the target density as close as possible and hence to have an acceptance rate as high as possible. At least, g should generally follow h , but with heavier tails [24, 57]. These guidelines for MH acceptance rates are in contrast to those prescribed for the more common random walk MH, in which the best convergence is generally obtained with acceptance rates between 20% and 50% [24, 58]. In the sequel, we discuss our proposed generating distribution both as an independence sampler as well as its use in an accept-reject algorithm.

3.3 Metropolis-within-Gibbs

It is often the case in practice that one or more of the full conditional distributions necessary to implement the Gibbs sampler are either not available or computationally prohibitive. In this situation

one can substitute an MH step to approximate a draw from the conditional distribution of interest. So-called ‘Metropolis-within-Gibbs’ algorithms [45] are such that each individual sub-chain is not irreducible with respect to the entire parameter space, since each only moves on a lower dimensional subspace [57]. With the remaining parameters held fixed, however, each MH sub-step does produce a valid Markov chain with stationary distribution equal to the full conditional distribution that is to be approximated. As such, running several MH updates in a subsampling step may improve convergence of the entire algorithm [47, 20, 14], but a single MH update for each full Gibbs scan is often done in practice. The transition kernel for the Metropolis-within-Gibbs chain is a cycle of transition kernels $K = K_1 \circ \dots \circ K_l$, where each K_i has the same stationary distribution, hence preserving the target distribution [72]. It is often the case that such cycles will be uniformly ergodic, leading to fast convergence.

4 Computationally Efficient Sampling for the Bayesian Inverse Problem

The joint posterior distribution of the model specified by equations (2), (3), and (4) is given by

$$\pi(\mathbf{x}, \mu, \sigma \mid \mathbf{b}) \propto \mu^{m/2+\alpha_\mu-1} \sigma^{n/2+\alpha_\sigma-1} \exp\left(-\frac{\mu}{2}\|\mathbf{A}\mathbf{x} - \mathbf{b}\|_2^2 - \frac{\sigma}{2}\|\mathbf{L}\mathbf{x}\|_2^2 - \beta_\mu\mu - \beta_\sigma\sigma\right). \quad (7)$$

Since \mathbf{x} is expected to be highly correlated in the posterior, it is desirable to update it all at once in a block Gibbs sampler. The full conditional distributions in this case are

$$\mathbf{x} \mid \mathbf{b}, \mu, \sigma \sim \mathcal{N}(\mathbf{x}_{\text{cond}}, \mathbf{\Gamma}_{\text{cond}}) \quad (8)$$

$$\mu \mid \mathbf{x}, \mathbf{b}, \sigma \sim \Gamma\left(m/2 + \alpha_\mu, \frac{1}{2}\|\mathbf{A}\mathbf{x} - \mathbf{b}\|_2^2 + \beta_\mu\right) \quad (9)$$

$$\sigma \mid \mathbf{x}, \mathbf{b}, \mu \sim \Gamma\left(n/2 + \alpha_\sigma, \frac{1}{2}\mathbf{x}^\top \mathbf{\Gamma}_{\text{pr}}^{-1} \mathbf{x} + \beta_\sigma\right), \quad (10)$$

where \mathbf{x}_{cond} and $\mathbf{\Gamma}_{\text{cond}}$ are as defined in Section 2. The block Gibbs sampling algorithm is given in Algorithm 2.

<p>Input: Full conditional distributions (8), (9), and (10), sample size N, burn-in period N_b. Output: Approximate sample from the posterior distribution of $\{\mathbf{x}_{(t)}, \mu_{(t)}, \sigma_{(t)}\}_{t=N_b+1}^N$.</p> <pre> 1 Initialize $\mathbf{x}_{(0)}$, $\mu_{(0)}$, and $\sigma_{(0)}$. 2 for $t = 1$ to N do 3 Draw $\mathbf{x}_{(t)} \sim \mathcal{N}(\mu_{(t-1)}\mathbf{\Gamma}_{\text{cond}}^{(t)}\mathbf{A}^\top \mathbf{b}, \mathbf{\Gamma}_{\text{cond}}^{(t)})$ where $\mathbf{\Gamma}_{\text{cond}}^{(t)} = (\mu_{(t-1)}\mathbf{A}^\top \mathbf{A} + \sigma_{(t-1)}\mathbf{\Gamma}_{\text{pr}}^{-1})^{-1}.$ 4 Draw $\mu_{(t)} \sim \Gamma(m/2 + \alpha_\mu, \beta_{\mu,t})$ where $\beta_{\mu,t} := \frac{1}{2}\ \mathbf{A}\mathbf{x}_{(t)} - \mathbf{b}\ _2^2 + \beta_\mu$. 5 Draw $\sigma_{(t)} \sim \Gamma(n/2 + \alpha_\sigma, \beta_{\sigma,t})$ where $\beta_{\sigma,t} := \frac{1}{2}\ \mathbf{L}\mathbf{x}_{(t)}\ _2^2 + \beta_\sigma$. 6 end </pre>

Algorithm 2: Block Gibbs sampling for the posterior density (7).

The computational cost per iteration of block Gibbs is dominated by the first step, sampling from the Gaussian distribution in line 3. While sampling from this Gaussian distribution is a very straightforward procedure, the fact that it is high-dimensional makes it very computationally intensive. To circumvent the computational burden, we propose approximating the samples from this distribution with a computationally cheap surrogate and correcting for the approximation via Metropolis

updates within each Gibbs scan. This approach facilitates much faster sampling while maintaining convergence to the joint distribution of interest, (7).

4.1 Approximating the target distribution

Samples from the distribution $\mathcal{N}(\mathbf{x}_{\text{cond}}, \mathbf{\Gamma}_{\text{cond}})$ may be generated as $\mathbf{x} = \mathbf{x}_{\text{cond}} + \mathbf{G}\boldsymbol{\epsilon}$, where $\boldsymbol{\epsilon} \sim \mathcal{N}(\mathbf{0}, \mathbf{I})$ and \mathbf{G} satisfies $\mathbf{\Gamma}_{\text{cond}} = \mathbf{G}\mathbf{G}^\top$. Forming the mean \mathbf{x}_{cond} and computing the random vector $\mathbf{G}\boldsymbol{\epsilon}$ involve expensive operations with the covariance matrix. By leveraging the low-rank nature of the forward operator \mathbf{A} , though, we are able to derive a fast proposal distribution for use in a MHwG algorithm.

For convenience, we suppress the dependence of covariance matrices on the iteration number. We first consider the covariance matrix $\mathbf{\Gamma}_{\text{cond}} = (\mu\mathbf{A}^\top\mathbf{A} + \sigma\mathbf{L}^\top\mathbf{L})^{-1}$ of the Gaussian conditional distribution in Algorithm 2 line 3. Factorizing this matrix so that

$$\mathbf{\Gamma}_{\text{cond}} = (\mathbf{L}^\top\mu\mathbf{L}^{-\top}\mathbf{A}^\top\mathbf{A}\mathbf{L}^{-1}\mathbf{L} + \sigma\mathbf{L}^\top\mathbf{L})^{-1} = \mathbf{L}^{-1}(\mu\mathbf{L}^{-\top}\mathbf{A}^\top\mathbf{A}\mathbf{L}^{-1} + \sigma\mathbf{I})^{-1}\mathbf{L}^{-\top}, \quad (11)$$

yields the so-called *prior-preconditioned Hessian transformation* [12, 17, 52, 62]. For highly ill-posed inverse problems such as those considered here, \mathbf{A} either has a rapidly decaying spectrum or is rank deficient. The same properties are also inherited by the matrix $\mathbf{L}^{-\top}\mathbf{A}^\top\mathbf{A}\mathbf{L}^{-1}$, which we approximate using a truncated eigenvalue decomposition,

$$\mathbf{L}^{-\top}\mathbf{A}^\top\mathbf{A}\mathbf{L}^{-1} \approx \mathbf{V}_k\mathbf{\Lambda}_k\mathbf{V}_k^\top, \quad (12)$$

where $\mathbf{V}_k \in \mathbb{R}^{n \times k}$ has orthonormal columns and $\mathbf{\Lambda}_k \in \mathbb{R}^{k \times k}$ is the diagonal matrix containing the $k \leq n$ largest eigenvalues of $\mathbf{L}^{-\top}\mathbf{A}^\top\mathbf{A}\mathbf{L}^{-1}$. If $\text{rank}(\mathbf{A}) = k$, then exact equality holds. The truncation parameter k controls the tradeoff between computational and memory costs and the sampling efficiency of the proposal distribution (i.e., the acceptance ratio).

Approximating \mathbf{x}_{cond} and $\mathbf{\Gamma}_{\text{cond}}$ We can approximate the conditional covariance matrix $\mathbf{\Gamma}_{\text{cond}}$ by substituting (12) into (11),

$$\hat{\mathbf{\Gamma}}_{\text{cond}} \equiv \mathbf{L}^{-1} \frac{1}{\sigma} (\mathbf{I} + \frac{\mu}{\sigma} \mathbf{V}_k \mathbf{\Lambda}_k \mathbf{V}_k^\top)^{-1} \mathbf{L}^{-\top}.$$

Using the Woodbury identity and the fact that \mathbf{V}_k has orthonormal columns, the right-hand side of the above equation becomes

$$\hat{\mathbf{\Gamma}}_{\text{cond}} = \frac{1}{\sigma} \mathbf{L}^{-1} (\mathbf{I} - \mathbf{V}_k \mathbf{D}_k \mathbf{V}_k^\top) \mathbf{L}^{-\top},$$

where $\mathbf{D}_k \equiv \text{diag}(\mu\lambda_j(\mu\lambda_j + \sigma)^{-1}) \in \mathbb{R}^{k \times k}$ is a diagonal matrix and λ_j , $1 \leq j \leq k$, are the diagonals of $\mathbf{\Lambda}_k$. To approximate the mean \mathbf{x}_{cond} , replace $\mathbf{\Gamma}_{\text{cond}}$ by $\hat{\mathbf{\Gamma}}_{\text{cond}}$ so that $\hat{\mathbf{x}}_{\text{cond}} = \mu\hat{\mathbf{\Gamma}}_{\text{cond}}\mathbf{A}^\top\mathbf{b}$. With these approximations, the proposal distribution for our proposed independence sampler is $\mathcal{N}(\hat{\mathbf{x}}_{\text{cond}}, \hat{\mathbf{\Gamma}}_{\text{cond}})$. The optimality of this low-rank approximation was studied in [69].

Sampling from the proposal distribution A factorization of the form $\hat{\mathbf{\Gamma}}_{\text{cond}} = \mathbf{G}\mathbf{G}^\top$ is necessary to sample from $\mathcal{N}(\hat{\mathbf{x}}_{\text{cond}}, \hat{\mathbf{\Gamma}}_{\text{cond}})$. It can be verified that

$$\mathbf{G} := \frac{1}{\sqrt{\sigma}} \mathbf{L}^{-1} (\mathbf{I} - \mathbf{V}_k \hat{\mathbf{D}}_k \mathbf{V}_k^\top),$$

with $\hat{\mathbf{D}}_k = \mathbf{I} \pm (\mathbf{I} - \mathbf{D}_k)^{1/2}$, satisfies $\hat{\mathbf{\Gamma}}_{\text{cond}} = \mathbf{G}\mathbf{G}^\top$, where the square root is taken componentwise. Since $\hat{\mathbf{D}}_k$ is diagonal and $k \ll n$, we obtain a computationally cheap way of generating draws from the high-dimensional proposal distribution $\mathcal{N}(\hat{\mathbf{x}}_{\text{cond}}, \hat{\mathbf{\Gamma}}_{\text{cond}})$, and use a Metropolis-Hastings step to correct for the approximation. This results in the Metropolis-Hastings-within-Gibbs (MHwG) independence sampling algorithm. See Section 4.3 for more details of the computational cost.

4.2 Acceptance ratio

In this subsection, we derive an explicit formula for evaluating the acceptance ratio for the MHwG algorithm and provide insight into the conditions for which the proposal distribution $\mathcal{N}(\hat{\mathbf{x}}_{\text{cond}}, \hat{\mathbf{\Gamma}}_{\text{cond}})$ closely approximates the target distribution $\mathcal{N}(\mathbf{x}_{\text{cond}}, \mathbf{\Gamma}_{\text{cond}})$. For simplicity, we drop the conditioning on \mathbf{b}, μ and σ . The target density is

$$h(\mathbf{x}) := \frac{1}{\sqrt{(2\pi)^n \det(\mathbf{\Gamma}_{\text{cond}})}} \exp\left(-\frac{1}{2}(\mathbf{x} - \mathbf{x}_{\text{cond}})^\top \mathbf{\Gamma}_{\text{cond}}^{-1}(\mathbf{x} - \mathbf{x}_{\text{cond}})\right), \quad (13)$$

and the proposal density, $q(\mathbf{x})$, replaces \mathbf{x}_{cond} by $\hat{\mathbf{x}}_{\text{cond}}$ and $\mathbf{\Gamma}_{\text{cond}}$ by $\hat{\mathbf{\Gamma}}_{\text{cond}}$ in the density $h(\mathbf{x})$. The following result gives a practical way to compute the acceptance ratio.

Proposition 1. *The MH acceptance ratio can be computed as $\eta(\mathbf{z}, \mathbf{x}) = w(\mathbf{z})/w(\mathbf{x})$, where*

$$w(\mathbf{x}) = \exp\left(-\frac{1}{2}\mathbf{x}^\top (\mathbf{\Gamma}_{\text{cond}}^{-1} - \hat{\mathbf{\Gamma}}_{\text{cond}}^{-1})\mathbf{x}\right).$$

Proof. See Appendix A. □

An efficient implementation and the cost of computing this ratio is discussed in Section 4.3.

Acceptance rate of MHwG The quality of the low-rank approximation to the target distribution can be seen through its relationship to the acceptance ratio of the MHwG sampler, given by the following Proposition.

Proposition 2. *The MH acceptance ratio can be simplified to*

$$\eta(\mathbf{z}, \mathbf{x}) = \exp\left(-\frac{\mu}{2} \sum_{j=k+1}^n \lambda_j \left[(\mathbf{v}_j^\top \mathbf{L}\mathbf{z})^2 - (\mathbf{v}_j^\top \mathbf{L}\mathbf{x})^2\right]\right). \quad (14)$$

Proof. See Appendix A. □

This Proposition asserts that the acceptance ratio is high when either μ is small or the discarded eigenvalues $\{\lambda_j\}_{j=k+1}^n$ are small. The dependence of the acceptance ratio on the eigenvectors can be seen explicitly by writing

$$(\mathbf{v}_j^\top \mathbf{L}\mathbf{z})^2 - (\mathbf{v}_j^\top \mathbf{L}\mathbf{x})^2 = [\mathbf{v}_j^\top \mathbf{L}(\mathbf{z} + \mathbf{x})] [\mathbf{v}_j^\top \mathbf{L}(\mathbf{z} - \mathbf{x})].$$

Thus, if $\mathbf{z} \pm \mathbf{x} \perp \mathbf{L}^\top \mathbf{v}_j$, then the acceptance ratio is 1. Furthermore, assuming that $\mathbf{z} = \hat{\mathbf{x}}_{\text{cond}} + \mathbf{G}\boldsymbol{\epsilon}_{\mathbf{z}}$ and $\mathbf{x} = \hat{\mathbf{x}}_{\text{cond}} + \mathbf{G}\boldsymbol{\epsilon}_{\mathbf{x}}$, this expression simplifies to $\boldsymbol{\epsilon}_{\mathbf{z}} - \mathbf{G}\boldsymbol{\epsilon}_{\mathbf{x}} \perp \mathbf{v}_j$.

While Proposition 2 provides insight into realizations of the acceptance ratio, the actual acceptance ratio is random. The expected behavior and variability of this quantity can be understood through Proposition 3. Define the constant

$$N_\ell := \exp\left(\frac{\mu^2}{2\sigma} \sum_{j=k+1}^n \frac{\ell\mu\lambda_j}{\ell\mu\lambda_j + \sigma} (\mathbf{b}^\top \mathbf{A}\mathbf{L}^{-1}\mathbf{v}_j)^2\right) \prod_{j>k} \left(1 + \frac{\ell\mu}{\sigma}\lambda_j\right)^{1/2}, \quad (15)$$

for integers $\ell \geq 1$.

Proposition 3. *Given the current state of the chain \mathbf{x} , the expected value and the variance of the acceptance ratio are given by*

$$\begin{aligned}\mu_\eta &:= \mathbb{E}_{\mathbf{z}|\mathbf{x}}[\eta(\mathbf{z}, \mathbf{x})] = \frac{1}{N_1 w(\mathbf{x})} \\ \sigma_\eta^2 &:= \mathbb{V}_{\mathbf{z}|\mathbf{x}}[\eta(\mathbf{z}, \mathbf{x})] = \frac{1}{w^2(\mathbf{x})} \left(\frac{1}{N_2} - \frac{1}{N_1^2} \right).\end{aligned}\tag{16}$$

Proof. See Appendix A. □

This result allows us to place probabilistic bounds on the deviation of the realized acceptance ratio from its expected value for a given low-rank approximation and current state \mathbf{x} . A straightforward application of Chebyshev's inequality [54] gives that the probability of deviation from expectation satisfies

$$\Pr_{\mathbf{z}|\mathbf{x}} \left(\left| \eta(\mathbf{z}, \mathbf{x}) - \frac{1}{N_1 w(\mathbf{x})} \right| \geq \epsilon \right) \leq \frac{1}{\epsilon^2 w^2(\mathbf{x})} \left(\frac{1}{N_2} - \frac{1}{N_1^2} \right),\tag{17}$$

where we have assumed that $w(\mathbf{x})$ is bounded from below; i.e., $w(\mathbf{x}) \geq \epsilon' > 0$. Thus, we can construct conditional prediction intervals about the realized acceptance rate. For instance, at any given state \mathbf{x} , $\Pr_{\mathbf{z}|\mathbf{x}}(\eta(\mathbf{z}, \mathbf{x}) \in [\mu_\eta \pm 4.47\sigma_\eta]) \geq 0.95$.

The result also gives additional insight into the average acceptance ratio. It is clear that if the eigenvalues $\{\lambda_j\}_{j=k+1}^n$ are zero, then the acceptance probability is 1. Likewise, if the eigenvalues are nonzero but small in magnitude, then the acceptance rate is close to 1. Further, consider the term $\mathbf{b}^\top \mathbf{A} \mathbf{L}^{-1} \mathbf{v}_j$ in (15) and the SVD of $\mathbf{A} \mathbf{L}^{-1} = \mathbf{U} \mathbf{\Sigma} \mathbf{V}^\top$. Then $\mathbf{b}^\top \mathbf{A} \mathbf{L}^{-1} \mathbf{v}_j = \sigma_j \mathbf{b}^\top \mathbf{u}_j$, where \mathbf{u}_j is the j th singular vector of $\mathbf{A} \mathbf{L}^{-1}$. Thus, the acceptance rate may be close to 1 even if the components of the measurement \mathbf{b} along the left singular vectors of $\mathbf{A} \mathbf{L}^{-1}$ are small. This is closely related to filter factors that arise in deterministic inverse problems [30].

Convergence and the Accept-Reject Algorithm The last Proposition shows that our proposed candidate generating distribution $q(\mathbf{x})$ bounds the target distribution up to a fixed constant, as a function of the remaining eigenvalues in the low-rank approximation.

Proposition 4. *The target density $h(\mathbf{x})$ (13) and the proposal density $q(\mathbf{x})$ can be bounded as $h(\mathbf{x}) \leq N_1 q(\mathbf{x})$ for all \mathbf{x} , where $N_1 \geq 1$ is given in (15).*

Proof. See Appendix A. □

Proposition 4 establishes that the subchain produced by our proposed sampler has stationary distribution $\pi(\cdot | \mathbf{b}, \mu, \sigma)$ and is *uniformly ergodic* by [57, Theorem 7.8];

$$\|K^p(\mathbf{x}, \cdot) - \pi(\cdot | \mathbf{b}, \mu, \sigma)\|_{TV} \leq 2(1 - N_1^{-1})^p \quad \forall \mathbf{x} \in \text{supp } \pi,$$

where $K^p(\mathbf{x}, \cdot)$ is the p -step transition kernel starting from \mathbf{x} and $\|\cdot\|_{TV}$ denotes the total variation norm. Thus, if one runs several sub-iterations of the MH independence sampler, the realizations will quickly converge to a draw from the true full conditional distribution. This convergence is faster as the remaining eigenvalues from the low-rank approximation become small, and is immediate when the remaining eigenvalues are zero.

Proposition 4 suggests also that the approximating distribution $q(\cdot)$ can be used in an accept-reject algorithm instead of the independence MH sampler. The expected number of candidate draws until one is accepted is N_1^{-1} , so that the sampling efficiency increases along with the rate at which the eigenvalues decay. The proof of this Proposition shows that $\det(\hat{\mathbf{\Gamma}}_{\text{cond}}) \geq \det(\mathbf{\Gamma}_{\text{cond}})$. But each determinant is the generalized variance of its distribution [36]. When there are non-zero eigenvalues left out of the low-rank approximation, the proposal density will have heavier tails than the target

density, a desirable property for a candidate distribution in a rejection algorithm [23]. Otherwise, the approximation is exact. We remark, however, that for a given candidate density g , an independence MH algorithm is superior to an accept-reject algorithm in terms of sampling efficiency [57, Lemma 7.9]. Therefore, in our simulation study in Section 5, we use the independence sampler instead of accept-reject. Our proposed MWwG algorithm is given in Algorithm 3.

Input: Full conditional distributions (8), (9), and (10), proposal distribution $q(\cdot \mid \mathbf{b}, \mu, \sigma)$, sample size N , burn-in period N_b .	
Output: Approximate sample from the posterior distribution (7) $\{\mathbf{x}_{(t)}, \mu_{(t)}, \sigma_{(t)}\}_{t=N_b+1}^N$.	
1	Initialize $\mathbf{x}_{(0)}$, $\mu_{(0)}$, and $\sigma_{(0)}$.
2	for $t = 1$ to N do
3	Draw \mathbf{x}_* from distribution with density $q(\cdot \mid \mathbf{b}, \mu_{(t-1)}, \sigma_{(t-1)})$.
4	if $u \leq \eta(\mathbf{x}_{(t-1)}, \mathbf{x}_*)$ then Set $\mathbf{x}_{(t)} = \mathbf{x}_*$. else Set $\mathbf{x}_{(t)} = \mathbf{x}_{(t-1)}$.
5	Draw $\mu_{(t)} \sim \Gamma(m/2 + \alpha_\mu, \beta_{\mu,t})$ where $\beta_{\mu,t} := \frac{1}{2} \ \mathbf{A}\mathbf{x}_{(t)} - \mathbf{b}\ _2^2 + \beta_\mu$.
6	Draw $\sigma_{(t)} \sim \Gamma(n/2 + \alpha_\sigma, \beta_{\sigma,t})$ where $\beta_{\sigma,t} := \frac{1}{2} \ \mathbf{L}\mathbf{x}_{(t)}\ _2^2 + \beta_\sigma$.
7	end

Algorithm 3: Metropolis-Hastings-within-Gibbs (MHwG) algorithm for sampling from the posterior distribution in (7).

4.3 Computational costs

Denote the computational cost of forming the matrix-vector product (referred to as matvec) with \mathbf{A} by $T_{\mathbf{A}}$, and the cost of matvec with \mathbf{L} and \mathbf{L}^{-1} as $T_{\mathbf{L}}$ and $T_{\mathbf{L}^{-1}}$ respectively. For simplicity, we assume the cost of the transpose operations of the respective matrices is the same as that of the original matrix.

The major cost of the sampler is the precomputation cost; i.e., constructing the low-rank approximation in (12). The standard approach for computing this low-rank approximation is to use a Krylov subspace solver (e.g., Lanczos method [60]) for computing eigenvalue decomposition. While it is difficult to estimate the cost of the the Krylov subspace method *a priori*, the cost is roughly 2 sets of matvecs with \mathbf{A} and \mathbf{L}^{-1} and an additional $\mathcal{O}(nk^2)$ operations. Alternatively, a numerically stable procedure is to compute the rank- k singular value decomposition $\mathbf{A}\mathbf{L}^{-1} \approx \mathbf{U}_k \mathbf{\Sigma}_k \mathbf{V}_k^\top$. Then the approximate low-rank decomposition can be computed as $\mathbf{L}^{-\top} \mathbf{A}^\top \mathbf{A} \mathbf{L}^{-1} \approx \mathbf{V}_k \mathbf{\Sigma}_k^2 \mathbf{V}_k^\top$. Efficient methods for computing the partial SVD can be found, for example, in [68]. Note that the quantities $\mathbf{A}^\top \mathbf{b}$ and $\mathbf{L}^{-\top} \mathbf{A}^\top \mathbf{b}$ can also be precomputed, and cost $T_{\mathbf{A}}$ and $T_{\mathbf{A}} + T_{\mathbf{L}^{-1}}$ flops respectively.

Operation	Formula	Cost
Precomputation	Equation (12)	$2k(T_{\mathbf{A}} + T_{\mathbf{L}^{-1}}) + \mathcal{O}(nk^2)$
Computing mean	$\hat{\mathbf{x}}_{\text{cond}} = \mu \hat{\mathbf{\Gamma}}_{\text{cond}} \mathbf{A}^\top \mathbf{b}$	$T_{\mathbf{L}^{-1}} + 4nk$
Generating sample	$\mathbf{x} \sim \mathcal{N}(\hat{\mathbf{x}}_{\text{cond}}, \hat{\mathbf{\Gamma}}_{\text{cond}})$	$T_{\mathbf{L}^{-1}} + 4nk$
Acceptance ratio	Proposition 1	$T_{\mathbf{A}} + T_{\mathbf{L}} + 2n(k+2)$

Table 1: Summary of computational costs of various steps in the MHwG algorithm.

The cost of computing the mean $\hat{\mathbf{x}}_{\text{cond}}$ involves the application of \mathbf{L}^{-1} and $(\mathbf{I} - \mathbf{V}_k \mathbf{D}_k \mathbf{V}_k^\top)$; together, this costs $T_{\mathbf{L}^{-1}} + 4nk$ flops. Similarly, the cost of $\mathbf{G}\epsilon$ is also $T_{\mathbf{L}^{-1}} + 4nk$ flops. The important point to note here is that generating a sample from the proposal distribution does not require a matvec with \mathbf{A} . This is useful for applications in which $T_{\mathbf{A}}$ can be extremely high. The computational cost of computing the acceptance ratio can be examined in light of Proposition 1. On each iteration, the weight $w(\mathbf{x})$ will already be available from the previous iteration, so we only need to compute

$w(\mathbf{z})$. We can simplify this expression as

$$\log w(\mathbf{z}) = -\mu \mathbf{z}^\top (\mathbf{A}^\top \mathbf{A} - \mathbf{L}^\top \mathbf{V}_k \mathbf{\Lambda}_k \mathbf{V}_k^\top \mathbf{L}) \mathbf{z}.$$

This computation requires one matvec with \mathbf{A} and \mathbf{L} each, two inner products and $4n$ flops, and an additional $2nk$ flops. Aside from the precomputational cost of the low-rank factorization, only the evaluation of the acceptance ratio requires accessing the forward operator \mathbf{A} . The resulting costs are summarized in Table 1.

4.4 Convergence Diagnostics

As discussed in Section 3, any MCMC procedure will generally *not* result in an immediate draw from the target distribution (unless the initial distribution is the stationary distribution), since the target is the limiting distribution. While it is very difficult to prove that a chain has converged to its limiting distribution, many diagnostic tools can be used to assess whether or not the chain is sufficiently close (e.g., [57], Chapter 12). We use these tools to assess the convergence of the chains obtained from our numerical illustrations in Section 5.

Common diagnostic tools used in practice are trace plots and potential scale reduction factors. Trace plots are graphical displays of the values of particular scalars θ_i versus the iteration number. When multiple chains are run, each starting from different, relatively dispersed initial values, a sign of convergence is when the realizations of the chains tend to the same part of the parameter space and overlap when superimposed on the trace plot. One can also use the trace plot of a single chain, looking for when the chain seems to “settle down” without moving from one part of the space to another. The latter approach is more susceptible to *pseudo-convergence* in which the chain gets trapped in a local mode of the target distribution, without fully exploring all of the high probability areas. Potential scale reduction factors (PSRFs), on the other hand, are quantitative measures which use the *within* chain variability and *between* chain variability (of three or more chains) to estimate the factor by which the variance of the current distribution of a parameter of interest might be reduced if the simulations were allowed to run indefinitely [25]. For a scalar estimand θ , the PSRF is

$$\hat{R} = \sqrt{\frac{\hat{\mathbb{V}}(\theta)}{W}}, \quad \hat{\mathbb{V}}(\theta) = \frac{N-1}{N}W + \frac{1}{N}B,$$

where W is the average within-chain variance of $m_c \geq 3$ chains, each of length N , and B is the between-chain variance. This quantity tends to 1 as $N \rightarrow \infty$, and $W \gg 1$ indicates the need to run the chain longer before approximate convergence is attained. A generalization of PSRFs to the multivariate case takes $\hat{R}_{MV} = (N-1)/N + \lambda_1(m_c+1)/m_c$, where λ_1 is the largest eigenvalue of $W_{MV}^{-1}B_{MV}/N$ and W_{MV} and B_{MV} are the within- and between-chain covariance matrices, respectively [11]. As in the scalar case, $\hat{R}_{MV} \rightarrow 1$ as $N \rightarrow \infty$.

5 Illustrations

Here we demonstrate our proposed approach on three simulated examples. The first example is a standard one dimensional deblurring problem in which we compare the performance of a fully Bayesian approach versus MAP estimation. The second and third examples are motivated by medical imaging applications. We compare the computational performance of block Gibbs sampling with our proposed low-rank MCMC approach, as well as demonstrate the competitive solutions obtained from using the posterior mean estimate evaluated using MCMC and from the MAP approach with regularization parameter determined from the posterior distribution.

5.1 One Dimensional Image Restoration

First, we consider the image reconstruction problem originally appearing in [66]. This is a one-dimensional image restoration problem in which the blurred image can be expressed as a Fredholm integral equation of the first kind. For this example, we use the implementation in the Matlab package **Regularization Tools** [29]. The integral is discretized via quadrature over $n = 512$ points, and we corrupt the observations with one percent noise, resulting in the model in (1) where $\epsilon \sim \mathcal{N}(\mathbf{0}, \mathbf{\Gamma})$ and $\mathbf{\Gamma} = 0.01^2 \|\mathbf{b}\|^2 \mathbf{I}$. The observed data \mathbf{b} and the true underlying function are displayed in Figure 1.

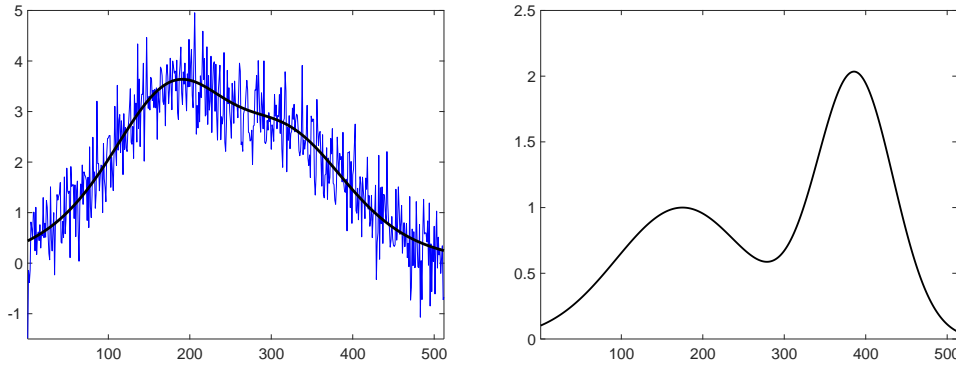


Figure 1: Observed data (left panel) and true solution (right panel) for the one-dimensional image restoration example. The solid black line in the left panel represents the noise-free observations \mathbf{Ax} .

To incorporate *a priori* information concerning the smoothness of the solution, we use a zero mean Gaussian process (GP) prior [63, 55], $f(\cdot) \sim \mathcal{GP}(0, \sigma^{-1}R(\cdot, \cdot))$. We take the correlation function to be in the power exponential family, $R(t_i, t_j) = \exp(-2|t_i - t_j|/\pi)$. The model is completed by specifying priors for the noise and GP precision parameters. In this case we use a relatively informative prior about the noise precision μ with $\alpha_\mu = \beta_\mu = 1$ so that $\mathbb{E}(\mu) = \mathbb{V}(\mu) = 1$, *a priori*. Similarly, we concentrate the GP precision about small values to reflect our prior knowledge concerning plausible values of the regularization parameter $\lambda = \sigma/\mu$. We take $\alpha_\sigma = 0.001$ and $\beta_\sigma = 10$ so that, *a priori*, $\mathbb{E}(\sigma) = 10^{-4}$ and $\mathbb{V}(\sigma) = 10^{-5}$.

Figure 4 displays the first 50 eigenvalues of the prior-preconditioned Hessian that is used in our proposed Metropolis-Hastings-within-Gibbs (MHwG) algorithm. We can see the poor conditioning of this problem in the quickly decaying spectrum of the matrix. Observe that most of the information is captured in the first ten eigenvalues or so. We set our proposal distribution by keeping the first $k = 25$ eigenvalues of the matrix.

We implement our proposed Metropolis-Hastings-within-Gibbs (MHwG) algorithm using three different chains run in parallel with different starting values to assess convergence. Each chain is run for $N = 2000$ iterations with the first $N_b = 500$ iterations discarded as a burn-in period. Convergence is assessed both graphically with trace plots of the three chains and quantitatively using potential scale reduction factors [25, 11]. After approximate convergence is attained, the output from the three chains is combined for a Monte Carlo sample size of 4500. In determining the regularization parameter for the MAP solution to this problem, we use ordinary leave-one-out cross validation (loo-CV) over a grid of plausible values. We compare this value with the posterior mean estimate calculated as $\hat{\lambda} = \hat{\sigma}/\hat{\mu}$.

Figure 2 displays the estimates of f using both the MAP approach as well as the posterior mean obtained via MCMC. The MAP estimator using the posterior mean for λ and the posterior mean of \mathbf{x} yield comparable solutions. In contrast, the cross-validated MAP estimator yields a considerably different solution, so that the two approaches are not equivalent. The posterior mean solutions are superior in terms of both relative error and root mean square error, as evident in Table 2. In addition

Estimator	RE	RMSE
MAP	0.3708	0.3702
Posterior Mean	0.3659	0.3652

Table 2: Relative error (RE) and root mean square error (RMSE) of the estimates for the one-dimensional image restoration example.

to the good performance of the point estimator, access to the full posterior distribution facilitates a complete quantification of uncertainty about the solution, something that is not possible under the conventional MAP approach. We see that the greatest uncertainty about the true image is at the boundaries of the domain, as expected.

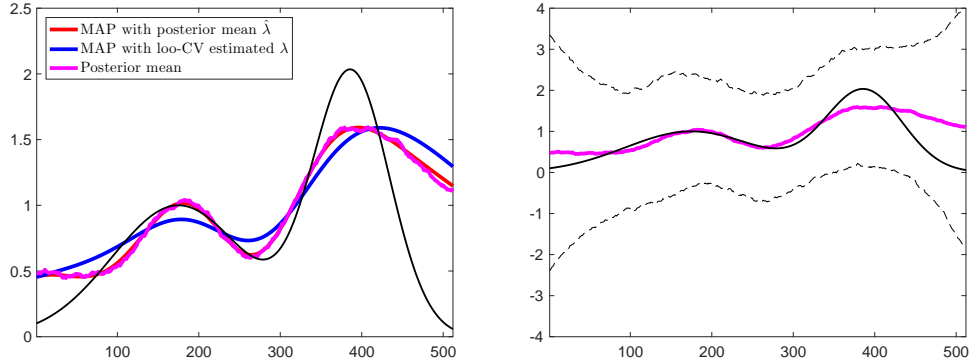


Figure 2: MAP estimates and posterior mean estimate for the one-dimensional image restoration example. In both panels, the black line is the true image. In the left panel, the blue line is the estimator obtained from loo-CV, the red line is the MAP estimator using the posterior mean estimate of regularization parameter, and the magenta line is the posterior mean solution. In the right panel, the posterior mean is plotted with approximate 95% pointwise error bounds given by the dashed lines.

Figure 3 displays the estimates of the marginal posterior densities for the precision parameters μ and σ . These are estimated using the MCMC samples collected with our proposed algorithm as described above. We see a larger variance in the noise precision parameter than in the prior precision parameter. Note that the marginal posterior of σ appears multimodal due to the highly correlated draws in the sampling chain, an issue which is known to occur in such ill-posed Bayesian inverse problems [9]. Combining samples from different chains yields a more complete picture of the posterior distribution.

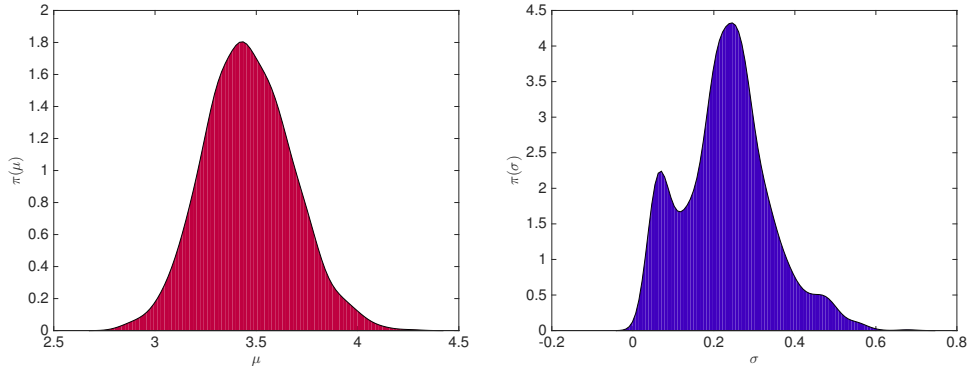


Figure 3: Estimated marginal posterior densities for μ (left panel) and σ (right panel) for the one-dimensional image restoration example.

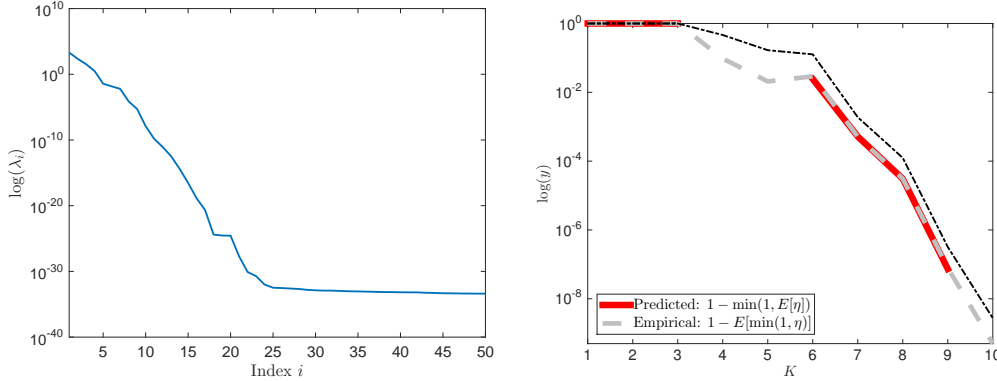


Figure 4: (Left) Spectrum of the prior-preconditioned Hessian matrix for the one-dimensional image restoration example. (Right) Rejection rates y computed with different eigenvalue truncations for the one-dimensional image restoration example, \log_{10} scale. Approximate 95% pointwise error upper bound given by the dashed line. Note that the lower bound for the pointwise error is negative and therefore not plotted.

To explore the effect on the acceptance ratios of the retained number of eigenvalues in the approximate proposal distribution, we repeat the above procedure over a range of truncation levels. We again implement our MHwG algorithm using three different chains in parallel with different starting values, each run for 2000 iterations. At each iteration, we compute the acceptance ratio using Proposition 2. We retain the last 500 samples from each chain for a total sample size of 1500, and retain also their corresponding acceptance ratios. We compare these with the average of the overall acceptance rates across the three chains. As more non-negligible eigenvalues are retained in the approximation, the acceptance ratios converge to 1. Retaining the first $k = 15$ or more eigenvalues results in acceptance ratios of 1 for all samples.

Lastly, we investigate the rejection rates as a function of the number of retained eigenvalues. We fix values for \mathbf{x}, μ, σ by selecting a sample at random from the 1500 sample set used previously. For each eigenvalue cutoff k , we generate 2000 samples from the proposal distribution $q(\mathbf{z})$, and we compute the acceptance ratio for each using Proposition 1. The number of rejected draws per 2000 proposal samples is compared to the expected rejection rate, $y = 1 - \min(\mathbb{E}_{\mathbf{z}|\mathbf{x}}[\eta(\mathbf{z}, \mathbf{x})], 1)$, with the expectation given in Proposition 3. Figure 4 displays the results as k increases. Note that the predicted rejection rate is zero in the case where $k = 4, 5$ because the expectation in this case is greater than one. In other cases, the empirical failure rate is comparable to the predicted failure rate. As the number of retained eigenvalues increases, both the mean and the variance in the rejection rate decrease to zero.

In this example, we are able to capture all of the salient features of the target distribution with very few eigenvalues, resulting in acceptance rates that rapidly approach 100%. This illustrates the potential of our proposed approach to greatly reduce the computational burden associated with drawing high-dimensional Gaussian random variables while still efficiently sampling from the full conditional distribution with few wasted iterations.

5.2 EEG Source Localization

In electroencephalography (EEG), neuronal activity is estimated by measuring electric potentials on the scalp generated as a result of such activity. An advantage of EEG is that it can estimate neural signals at a very high temporal resolution (on the millisecond scale). On the other hand, the inverse problem of determining the location of the neuronal activity that generates the EEG signal is formidable. Since the signals originate from within the three-dimensional brain volume yet are recorded along the two-dimensional surface of the scalp, there is a considerable loss of spatial

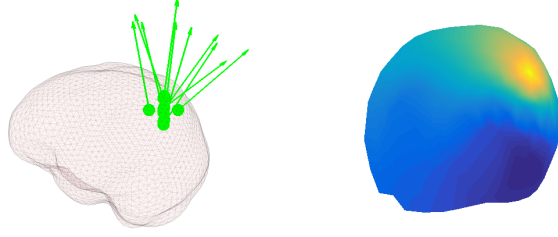


Figure 5: Simulated source dipoles (left) and measured scalp potentials (right) for the EEG example. The arrows in the left panel indicate strength and orientation of the dipoles.

resolution. Moreover, the neurophysiology of the human brain and surrounding tissue, particularly the poor conductivity of the skull, pose additional challenges [48]. Here we focus on source localization from scalp potentials measured at a single point in time.

The current per unit volume of the brain can be approximated as a dipole moment with a strength and orientation, denoted $\mathbf{P}(\mathbf{r})$, where \mathbf{r} is the vector indexing location in the brain. The measured scalp potential is then obtained as the sum (integral) of all the current sources throughout the brain volume that contribute to the signal, $\Phi(\mathbf{s}) = \int_B \mathcal{G}_H(\mathbf{s}, \mathbf{r}) \mathbf{P}(\mathbf{r}) dV(\mathbf{r})$, where \mathcal{G}_H is a Green's function representing the volume conduction of current passing through the head tissue and \mathbf{s} indexes scalp location. The Green's function is typically estimated numerically using the Boundary Element Method or the Finite Element Method. Discretization of the integral equation and the measurement error encountered in practice lead to the model $\mathbf{d} = \mathbf{A}_L \mathbf{s} + \epsilon$ where $\mathbf{d} \in \mathbb{R}^m$ is the vector of observed electrode potentials, $\mathbf{s} \in \mathbb{R}^n$ is the vector of amplitudes of current sources at each of n locations along the intracerebral source grid, and ϵ is Gaussian noise. The forward model \mathbf{A}_L is called the leadfield matrix. The discretization of the source grid is typically such that $n > m$ so that the inverse problem is ill-posed.

We simulate a cluster of ten source dipoles at a randomly chosen location in the brain volume. A realistic head volume conduction model estimated via Boundary Element Method is used to propagate the simulated sources to the surface potentials and to create the leadfield matrix. Noise with a maximum strength of 17% of the signal strength is added to the scale potentials to corrupt the observations. We suppose that the data are collected at $m = 257$ electrodes and the source grid is discretized to have dimension $n = 1261$. The simulated dipoles and scalp potentials are displayed in Figure 5. The data along with all graphical displays are created using the `FieldTrip` Matlab toolbox [49] and software freely available online [27].

For a fully Bayesian solution to the inverse problem, we take the prior on \mathbf{s} to be $\mathcal{N}(\mathbf{0}, \sigma^{-1} \mathbf{I})$ so that the EEG inverse solution is analogous to the conventional Tikhonov regularization advocated by Hauk [32]. We again choose the parameters in the Gamma priors so that μ is mildly concentrated about 1 with $\alpha_\mu = \beta_\mu = 1$ and σ is concentrated about 10^{-6} with $\alpha_\sigma = 0.01$ and $\beta_\sigma = 100$. We simulate the posterior distribution using both conventional block Gibbs sampling and our proposed low-rank MHwG algorithm. For both algorithms, three chains are run in parallel using dispersed initial values. Each chain uses 2000 iterations, discarding the first 500 draws as a burn-in period. In this case, the rank of the forward model \mathbf{A}_L is $257 < 1261$, so we retain only the 257 non-zero eigenvalues while maintaining an acceptance probability of one in the MHwG algorithm. The computations are done on a Dell Precision T3600 Windows 7 machine with 64GB RAM and Intel Xeon 3.30GHz processor.

Table 3 displays the potential scale reduction factors obtained from our proposed low-rank MHwG approach, and Figure 6 displays trace plots of the regularization parameter $\lambda = \sigma/\mu$. We remark that, since we are discarding only the zero eigenvalues in the low-rank approximation, our approach is identical to block Gibbs in terms of convergence behavior. As evident in Figure 7, the approximate

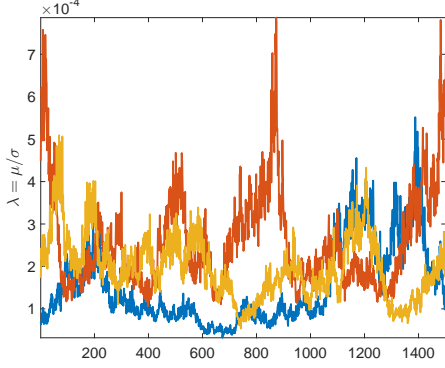


Figure 6: Trace plots of three realized chains of the regularization parameter $\lambda = \sigma/\mu$ obtained from the proposed MHwG algorithm in the EEG example.

Parameter	PSRF
μ	1.00
σ	1.041
\mathbf{s}	1.577

Table 3: Potential scale reduction factors (PSRF) for the parameters in Bayesian model for source localization in the EEG example. Since \mathbf{s} is of dimension 1261, we use the multivariate PSRF [11].

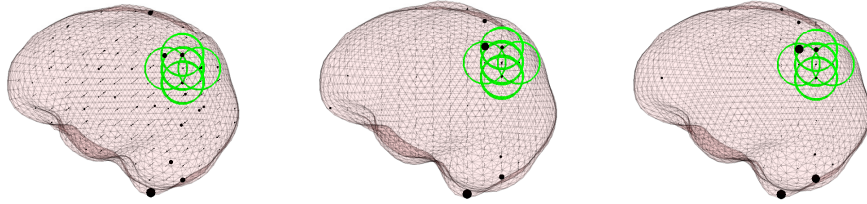


Figure 7: Solutions to the EEG inverse problem using block Gibbs (left panel), Metropolis-Hastings-within-Gibbs (middle panel), and MAP (right panel). Black dots indicate sources identified by the solution. Green circles indicate the true source dipoles in the simulated data

posterior mean calculated from either MCMC algorithm yields a solution very similar to the MAP estimator, where we use the posterior means of μ and σ to calculate λ .

A difference between the block Gibbs approach and our proposed approach is that by taking advantage of the low-rank structure in the precision matrix, we are able to reduce the total computation time by an order of magnitude, as displayed in Table 4. In this case, we attain a 97% improvement in overall computation time for the same number of MCMC iterations. There also is a dramatic improvement in sampling efficiency. Table 4 displays the *cost per effective sample* (CES) [19] of the regularization parameter obtained from both algorithms. This quantity is defined as $CES = \kappa\tau/N$ where τ is the total computation time, N is the length of the Markov chain, and κ is the integrated autocorrelation time [14] used in calculating the effective sample size from the output [38]. We see that our proposed algorithm is able to obtain a solution competitive with the MAP estimator along with measures of uncertainty afforded by the entire posterior distribution, all with much less computational effort than block Gibbs sampling.

Algorithm	Wall Time (s)	CES
Block Gibbs	610.714	82.770
MHwG	19.412	3.112

Table 4: Total computation time for block Gibbs and the proposed low-rank Metropolis-Hastings-within-Gibbs (MHwG) algorithms for simulating the posterior distribution in the EEG example. Also reported is the cost per effective sample of the regularization parameter obtained from the MCMC output of block Gibbs sampling and the proposed MHwG approach for the EEG example.

Estimator	RE	RMSE
MAP	0.4106	0.1006
Posterior Mean	0.4110	0.1007

Table 5: Relative error (RE) and root mean squared error (RMSE) of the two point estimators of the true image in the CT example.

5.3 CT Image Reconstruction

Computed x-ray tomography (CT) is a common medical imaging modality in which x-rays are passed through a body from a source to a sensor along parallel lines indexed by an angle ω and offset y with respect to a fixed coordinate system and origin. The intensities of the rays are attenuated according to an unknown absorption function as they pass through tissue. The attenuated intensity I is recorded while the lines are rotated around the origin so that

$$I(S) = I(0) \exp \left\{ - \int_0^S \alpha(x(s)) \, ds \right\},$$

where $s = 0$ is the source of the x-ray, $s = S$ is the receiver location, $x(\cdot)$ indicates the line position, and α is the absorption function. Typically, a transformation of the intensities comprise the observed data, yielding the Radon transform model for CT [37, 6], $z(\omega, y) = \int_{L(\omega, y)} \alpha(x(s)) \, ds$, where $L(\omega, y)$ is the line along which the x-ray passes through the body. Such data are called sinograms. The inverse problem is to reconstruct the absorption function, which provides an image of the scanned body. Discretization of the integral yields the model in (1). Like the EEG example, this is typically an underdetermined system with infinitely many solutions, resulting in an ill-posed inverse problem.

We take as our target image the Shepp-Logan phantom [67]. The forward model \mathbf{A} is implemented in Matlab using code available online [5]. The data are simulated by adding Gaussian noise with variance $0.01^2 \|\mathbf{A}\mathbf{x}\|_\infty^2$. Here, the target α is discretized to a relatively fine grid of size 128×128 so that $\dim(\mathbf{x}) = 16,384$ and we suppose that the data are observed over lines and angles such that $\dim(\mathbf{b}) = 5000$. Here, $\text{rank}(\mathbf{A}) = 5000 \ll \dim(\mathbf{x})$ so that we retain only the 5000 non-zero eigenvalues in the low-rank approximation to the prior preconditioned Hessian. We enforce smoothness as prior knowledge on \mathbf{x} by choosing $\mathbf{L} = -\Delta + \delta \mathbf{I}$, where $-\Delta$ is the discrete Laplacian and δ is a small constant to ensure positive definiteness [37]. The prior specifications on μ and σ are similar to those in the EEG example in Subsection 5.2, concentrating μ about 1 and σ about 10^{-6} *a priori*. We simulate a single Markov chain using the MCMC algorithm with our proposed low-rank approximation for 2000 iterations, discarding the first 1000 as a burn-in period so that we have a Monte Carlo sample size of 1000 from the approximate posterior distribution.

The total computation time for our sampling approach on a desktop running Windows 10 (16GB RAM, Intel Core i3-3220 3.30GHz processor) is 2748.7 s, or about forty-five minutes. This is noteworthy since the algorithm involves repeatedly updating a nontrivial covariance matrix and sampling from a sixteen-thousand dimensional Gaussian distribution. Our approach is much more feasible than a block Gibbs sampler for which such computational demands are prohibitively expensive. In addition, retaining all of the nonzero eigenvalues means we are sampling from the exact conditional distribution (with an acceptance rate of 100%) and so the statistical efficiency is equivalent to the Gibbs sampler. Again, we find that using the posterior mean as an estimate of the true image yields results competitive with the solution obtained from the MAP estimator, where the regularization parameter is determined from the MCMC output. The similarity between the two estimates is evident in Table 5, which displays the errors of the two approaches. The reconstructed images from both approaches are displayed in Figure 8.

These simulation results illustrate the ability of fully Bayesian solutions to the inverse problem to perform competitively with the deterministic MAP solution. Access to the full posterior distribution makes available more point estimators of the solution along with a set of plausible values of the

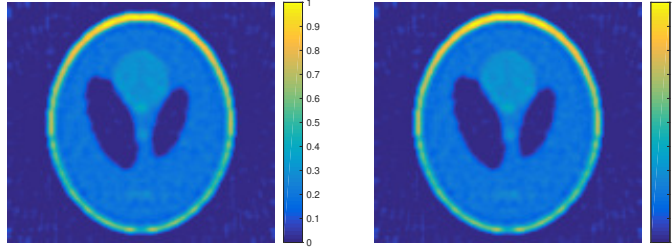


Figure 8: MAP estimate (left panel) and posterior mean (right panel) of the true image in the CT image reconstruction example.

regularization parameter for the MAP estimator. When approximating the posterior distribution via Markov chain Monte Carlo, the bottleneck is in repeatedly sampling high-dimensional Gaussian random variables. By exploiting the low-rank structure of the preconditioned Hessian of the forward model, we are able to substantially reduce the computational burden compared to block Gibbs sampling. Further, the computational gain does not sacrifice sampling efficiency. Even when the forward model is of full row rank, we illustrate the potential for efficiency gains using the proposed low-rank proposal approach, provided the system is underdetermined.

6 Discussion

In this work we propose a computationally efficient MCMC sampling algorithm for high-dimensional linear Bayesian inverse problems. We adopt a hierarchical Gaussian model in which the noise precision μ and the prior precision parameter σ are unknown. Sampling from the joint posterior with standard block Gibbs is computationally burdensome due to the dimensionality of \mathbf{x} , since drawing from the full conditional involves expensive operations with the covariance matrix.

Our proposed Metropolis-Hastings-within-Gibbs independence sampler uses a proposal distribution constructed via low-rank approximation to the preconditioned Hessian. This allows us to draw the full-dimensional parameters from the posterior efficiently. We show that the sampling efficiency is nearly one when the magnitudes of the discarded eigenvalues of the Hessian are small, a feature of severely ill-posed problems. We illustrate our approach on three simulated examples, showing that our proposed MCMC approach is computationally effective and yields reconstructions of similar quality to deterministic approaches, while also offering a means for quantifying the uncertainty in the parameters as well as automated regularization parameter selection.

One limitation of our approach is that the prior precision parameter is correlated with the spatial unknowns \mathbf{x} in the MCMC algorithm, and this correlation increases as the mesh refinement increases [1]. Methods to address this issue are proposed in [19, 9]. Combining our efficient sampler with these approaches is possibly an interesting avenue of future research.

7 Acknowledgements

Much of this work was done while the first author was a Visiting Research Fellow at the Statistical and Applied Mathematical Sciences Institute (SAMSI). This material is based upon work partially supported by the National Science Foundation under Grant DMS-1127914 to SAMSI. The authors also would like to thank Duy Thai, Vered Madar, and Ray Falk for useful conversations.

A Proofs

Proof of Proposition 1. Consider

$$\frac{h(\mathbf{x})}{q(\mathbf{x})} = \sqrt{\frac{\det(\hat{\mathbf{\Gamma}}_{\text{cond}})}{\det(\mathbf{\Gamma}_{\text{cond}})}} \hat{w}(\mathbf{x}),$$

where

$$\hat{w}(\mathbf{x}) := \exp\left(-\frac{1}{2}\|\mathbf{x} - \mathbf{x}_{\text{cond}}\|_{\mathbf{\Gamma}_{\text{cond}}^{-1}}^2 + \frac{1}{2}\|\mathbf{x} - \hat{\mathbf{x}}_{\text{cond}}\|_{\hat{\mathbf{\Gamma}}_{\text{cond}}^{-1}}^2\right).$$

and $\|\mathbf{w}\|_{\mathbf{M}} := \sqrt{\mathbf{w}^\top \mathbf{M} \mathbf{w}}$, a valid vector norm when \mathbf{M} is positive definite. With this definition, the acceptance ratio simplifies to $\eta(\mathbf{z}, \mathbf{x}) = \hat{w}(\mathbf{z})/\hat{w}(\mathbf{x})$. We can further simplify $\hat{w}(\mathbf{x})$ with

$$\begin{aligned} \log \hat{w}(\mathbf{x}) &= -\frac{1}{2}(\mathbf{x} - \mu \mathbf{\Gamma}_{\text{cond}} \mathbf{A}^\top \mathbf{b})^\top \mathbf{\Gamma}_{\text{cond}}^{-1} (\mathbf{x} - \mu \mathbf{\Gamma}_{\text{cond}} \mathbf{A}^\top \mathbf{b}) \\ &\quad + \frac{1}{2}(\mathbf{x} - \mu \hat{\mathbf{\Gamma}}_{\text{cond}} \mathbf{A}^\top \mathbf{b})^\top \hat{\mathbf{\Gamma}}_{\text{cond}}^{-1} (\mathbf{x} - \mu \hat{\mathbf{\Gamma}}_{\text{cond}} \mathbf{A}^\top \mathbf{b}), \\ &= -\frac{1}{2}\left(\mathbf{x}^\top \mathbf{\Gamma}_{\text{cond}}^{-1} \mathbf{x} + \mu^2 \mathbf{b}^\top \mathbf{A} \mathbf{\Gamma}_{\text{cond}} \mathbf{A} \mathbf{b}\right) \\ &\quad + \frac{1}{2}\left(\mathbf{x}^\top \hat{\mathbf{\Gamma}}_{\text{cond}}^{-1} \mathbf{x} + \mu^2 \mathbf{b}^\top \mathbf{A} \hat{\mathbf{\Gamma}}_{\text{cond}} \mathbf{A} \mathbf{b}\right). \end{aligned}$$

Some algebra shows that $\hat{w}(\mathbf{z})/\hat{w}(\mathbf{x}) = w(\mathbf{z})/w(\mathbf{x})$ and, therefore, the MH acceptance ratio simplifies to the desired result. \square

Proof of Proposition 2. The difference between the true and the approximate covariance matrices can be expressed as

$$\begin{aligned} \mathbf{\Gamma}_{\text{cond}}^{-1} - \hat{\mathbf{\Gamma}}_{\text{cond}}^{-1} &= \mu \mathbf{A}^\top \mathbf{A} + \sigma \mathbf{L}^\top \mathbf{L} - \left(\mu \mathbf{L}^\top \mathbf{V}_k \mathbf{\Lambda}_k \mathbf{V}_k \mathbf{L} + \sigma \mathbf{L}^\top \mathbf{L}\right), \\ &= \mu \mathbf{L}^\top \left(\mathbf{L}^{-\top} \mathbf{A}^\top \mathbf{A} \mathbf{L}^{-1} - \mathbf{V}_k \mathbf{\Lambda}_k \mathbf{V}_k\right) \mathbf{L}, \\ &= \mu \mathbf{L}^\top \left(\sum_{j=k+1}^n \lambda_j \mathbf{v}_j \mathbf{v}_j^\top\right) \mathbf{L}. \end{aligned}$$

The acceptance ratio is given by (14), where $w(\mathbf{x})$ simplifies to

$$\log w(\mathbf{x}) = -\frac{\mu}{2} \sum_{j=k+1}^n \lambda_j (\mathbf{v}_j^\top \mathbf{L} \mathbf{x})^2 \leq 0. \quad \square$$

We now reproduce a result from [63, Lemma B.1.1.].

Lemma 1. *Suppose \mathbf{M} is symmetric positive definite. Then,*

$$\int_{\mathbb{R}^n} \exp\left(-\frac{1}{2} \mathbf{z}^\top \mathbf{M} \mathbf{z} + \mathbf{J}^\top \mathbf{z}\right) d\mathbf{z} = \frac{(2\pi)^{n/2}}{\det(\mathbf{M})^{1/2}} \exp\left(\frac{1}{2} \mathbf{J}^\top \mathbf{M}^{-1} \mathbf{J}\right).$$

We next present a lemma on the moments of the acceptance ratio.

Lemma 2. *Let N_ℓ be defined as in (15). The moments of the acceptance ratio are*

$$\mathbb{E}_{\mathbf{z}|\mathbf{x}}[\eta^\ell(\mathbf{z}, \mathbf{x})] = \frac{1}{N_\ell w^\ell(\mathbf{x})}.$$

Proof of Lemma 2. The proof proceeds in four steps.

1. *Simplifying* $\mathbb{E}_{\mathbf{z}|\mathbf{x}}[w^m(\mathbf{z})]$. We focus on $\mathbb{E}_{\mathbf{z}|\mathbf{x}}[w^m(\mathbf{z})]$. In integral form, this is

$$\int_{\mathbb{R}^n} w^m(\mathbf{z}) q(\mathbf{z}) d\mathbf{z} = \frac{\exp\left(-\frac{1}{2}(\hat{\mathbf{x}}_{\text{cond}})^\top \hat{\mathbf{\Gamma}}_{\text{cond}}^{-1} \hat{\mathbf{x}}_{\text{cond}}\right)}{(2\pi)^{n/2} \det(\hat{\mathbf{\Gamma}}_{\text{cond}})^{1/2}} \int_{\mathbb{R}^n} \exp\left(-\frac{1}{2} \mathbf{z}^\top \mathbf{M} \mathbf{z} + \mathbf{J}^\top \mathbf{z}\right) d\mathbf{z},$$

where, by using $\hat{\mathbf{x}}_{\text{cond}} = \mu \hat{\mathbf{\Gamma}}_{\text{cond}} \mathbf{A}^\top \mathbf{b}$, we obtain

$$\mathbf{M} \equiv \ell \mathbf{\Gamma}_{\text{cond}}^{-1} + (1 - \ell) \hat{\mathbf{\Gamma}}_{\text{cond}}^{-1}, \quad \text{and} \quad \mathbf{J} \equiv \hat{\mathbf{\Gamma}}_{\text{cond}}^{-1} \hat{\mathbf{x}}_{\text{cond}} = \mu \mathbf{A}^\top \mathbf{b}.$$

Applying Lemma 1 and rearranging, we get

$$\mathbb{E}_{\mathbf{z}|\mathbf{x}}[w^\ell(\mathbf{z})] = \frac{\exp\left(\frac{\mu^2}{2} (\mathbf{A}^\top \mathbf{b})^\top (\mathbf{M}^{-1} - \hat{\mathbf{\Gamma}}_{\text{cond}}) \mathbf{A}^\top \mathbf{b}\right)}{\det(\mathbf{M})^{1/2} \det(\hat{\mathbf{\Gamma}}_{\text{cond}})^{1/2}}. \quad (18)$$

We focus on the numerator and denominator separately.

2. *Denominator of (18).* Note that

$$\mathbf{M} = \mathbf{L}^\top \left(\mu \sum_{j=1}^k \lambda_j \mathbf{v}_j \mathbf{v}_j^\top + \ell \mu \sum_{j=k+1}^n \lambda_j \mathbf{v}_j \mathbf{v}_j^\top + \sigma \mathbf{I} \right) \mathbf{L}.$$

Using properties of determinants, we can show that

$$\det(\mathbf{M}) = \sigma^n \det(\mathbf{L})^2 \prod_{j=1}^k \left(1 + \frac{\mu}{\sigma} \lambda_j\right) \prod_{j=k+1}^n \left(1 + \frac{\ell \mu}{\sigma} \lambda_j\right), \quad \det(\hat{\mathbf{\Gamma}}_{\text{cond}}^{-1}) = \sigma^n \det(\mathbf{L})^2 \prod_{j=1}^k \left(1 + \frac{\mu}{\sigma} \lambda_j\right).$$

Combining these results, the denominator of (18) becomes

$$\det(\mathbf{M})^{1/2} \det(\hat{\mathbf{\Gamma}}_{\text{cond}})^{1/2} = \sqrt{\frac{\det(\mathbf{M})}{\det(\hat{\mathbf{\Gamma}}_{\text{cond}})}} = \prod_{j>k} \left(1 + \frac{\ell \mu}{\sigma} \lambda_j\right)^{1/2}.$$

3. *Numerator of (18).* Consider $\mathbf{M}^{-1} - \hat{\mathbf{\Gamma}}_{\text{cond}}$. Using the Woodbury matrix identity,

$$\begin{aligned} \mathbf{M}^{-1} - \hat{\mathbf{\Gamma}}_{\text{cond}} &= \left(\ell \mathbf{\Gamma}_{\text{cond}}^{-1} + (1 - \ell) \hat{\mathbf{\Gamma}}_{\text{cond}}^{-1} \right)^{-1} - \hat{\mathbf{\Gamma}}_{\text{cond}}, \\ &= \frac{1}{\sigma} \mathbf{L}^{-1} \left(\mathbf{I} - \sum_{j=1}^k \frac{\mu \lambda_j}{\mu \lambda_j + \sigma} \mathbf{v}_j \mathbf{v}_j^\top - \sum_{j=k+1}^n \frac{\ell \mu \lambda_j}{\ell \mu \lambda_j + \sigma} \mathbf{v}_j \mathbf{v}_j^\top \right)^\top \mathbf{L}^{-\top} \\ &\quad - \frac{1}{\sigma} \left(\mathbf{I} - \sum_{j=1}^k \frac{\mu \lambda_j}{\mu \lambda_j + \sigma} \mathbf{v}_j \mathbf{v}_j^\top \right)^\top \mathbf{L}^{-\top}, \\ &= -\frac{1}{\sigma} \sum_{j=k+1}^n \frac{\ell \mu \lambda_j}{\ell \mu \lambda_j + \sigma} \mathbf{L}^{-1} \mathbf{v}_j \mathbf{v}_j^\top \mathbf{L}^{-\top}. \end{aligned}$$

Therefore, the numerator is

$$\exp\left(\frac{\mu^2}{2} (\mathbf{A}^\top \mathbf{b})^\top (\mathbf{M}^{-1} - \hat{\mathbf{\Gamma}}_{\text{cond}}) \mathbf{A}^\top \mathbf{b}\right) = \exp\left(-\frac{\mu^2}{2\sigma} \sum_{j=k+1}^n \frac{\ell \mu \lambda_j}{m \mu \lambda_j + \sigma} (\mathbf{b}^\top \mathbf{A} \mathbf{L}^{-1} \mathbf{v}_j)^2\right).$$

4. *Combining intermediate results.* Substituting the results of Steps 2 and 3 into (18) gives $\mathbb{E}_{\mathbf{z}|\mathbf{x}}[w^\ell(\mathbf{z})] = \frac{1}{N_\ell}$, where N_ℓ is defined in (15). The proof readily follows because $\mathbb{E}_{\mathbf{z}|\mathbf{x}}[\eta^\ell(\mathbf{z}, \mathbf{x})] = \mathbb{E}_{\mathbf{z}|\mathbf{x}}[w^\ell(\mathbf{z})]/w^\ell(\mathbf{x})$. \square

Proof of Proposition 3. From Lemma 2, we have $\mathbb{E}_{\mathbf{z}|\mathbf{x}}[\eta^\ell(\mathbf{z}, \mathbf{x})] = \frac{1}{N_\ell w^\ell(\mathbf{x})}$. The first result of (16) follows immediately by setting $\ell = 1$. The second result follows from the fact that $\text{Var}[X] = \mathbb{E}[X^2] - (\mathbb{E}[X])^2$ for any random variable X with finite second moment. We conclude the proof using the first result of (16) and applying Lemma 2 with $\ell = 2$. \square

Proof of Proposition 4. From the proof of Proposition 1,

$$\frac{h(\mathbf{x})}{q(\mathbf{x})} = \sqrt{\frac{\det(\hat{\mathbf{\Gamma}}_{\text{cond}})}{\det(\mathbf{\Gamma}_{\text{cond}})}} w(\mathbf{x}) \exp\left(-\frac{\mu^2}{2} \mathbf{b}^\top \mathbf{A}(\mathbf{\Gamma}_{\text{cond}} - \hat{\mathbf{\Gamma}}_{\text{cond}}) \mathbf{A}^\top \mathbf{b}\right).$$

From the proof of Lemma 2, $\mathbf{M}^{-1} = \mathbf{\Gamma}_{\text{cond}}$ when $\ell = 1$. Comparing terms with (18), this gives us $h(\mathbf{x}) = N_1 q(\mathbf{x}) w(\mathbf{x})$, where N_1 is defined in (15). From the proof of Proposition 2, $\log w(\mathbf{x}) \leq 0$, and therefore $w(\mathbf{x}) \leq 1$. The desired result follows. Note that the bound is tight because $w(\mathbf{0}) = 1$. \square

References

- [1] S. Agapiou, J. M. Bardsley, O. Papaspiliopoulos, and A. M. Stuart. Analysis of the Gibbs sampler for hierarchical inverse problems. *SIAM/ASA J. Uncertain. Quantif.*, 2(1):511–544, 2014.
- [2] S. Ambikasaran, A. K. Saibaba, E. F. Darve, and P. K. Kitanidis. Fast algorithms for Bayesian inversion. In *Computational Challenges in the Geosciences*, pages 101–142. Springer, 2013.
- [3] K. E. Andersen, S. P. Brooks, and M. B. Hansen. Bayesian inversion of geoelectrical resistivity data. *J. R. Stat. Soc. Ser. B. Stat. Methodol.*, 65(3):619–642, 2003.
- [4] S. Banerjee, A. E. Gelfand, A. O. Finley, and H. Sang. Gaussian predictive process models for large spatial data sets. *J. R. Stat. Soc. Ser. B. Stat. Methodol.*, 70(4):825–848, 2008.
- [5] J. M. Bardsley. WMRNSD for medical imaging examples. <http://www.math.umd.edu/bardsley/codes.html>. Accessed: 2016-06-23.
- [6] J. M. Bardsley. Applications of nonnegatively constrained iterative method with statistically based stopping rules to CT, PET, and SPECT imaging. *Electron. Trans. Numer. Anal.*, 38:34–43, 2011.
- [7] J. M. Bardsley. MCMC-based image reconstruction with uncertainty quantification. *SIAM J. Sci. Comput.*, 34(3):A1316–A1332, 2012.
- [8] J. M. Bardsley, M. Howard, and J. G. Nagy. Efficient MCMC-based image deblurring with Neumann boundary conditions. *Electron. Trans. Numer. Anal.*, 40:476–488, 2013.
- [9] J. M. Bardsley, K. T. Joyce, and A. Luttman. Partially Collapsed Gibbs Samplers for Linear Inverse Problems and Applications to X-ray Imaging. *Manuscript in submission*, 2016.
- [10] J. M. Bardsley and A. Luttman. A Metropolis-Hastings method for linear inverse problems with Poisson likelihood and Gaussian prior. *Int. J. Uncertain. Quantif.*, 6(1):35–55, 2016.
- [11] S. P. Brooks and A. Gelman. General methods for monitoring convergence of iterative simulations. *J. Comput. Graph. Statist.*, 7(4):434–455, 1998.

- [12] T. Bui-Thanh, O. Ghattas, J. Martin, and G. Stadler. A computational framework for infinite-dimensional Bayesian inverse problems part i: The linearized case, with application to global seismic inversion. *SIAM J. Sci. Comput.*, 35(6):A2494–A2523, 2013.
- [13] D. Calvetti, J. P. Kaipio, and E. Somersalo. Inverse Problems in the Bayesian Framework. *Inverse Problems*, 30(11), 2014.
- [14] B. P. Carlin and T. A. Louis. *Bayesian Methods for Data Analysis*. Chapman & Hall/CRC, Boca Raton, 3rd edition, 2009.
- [15] J. Chung, J. G. Nagy, and D. P. O’Leary. A weighted GCV method for Lanczos hybrid regularization. *Electron. Trans. Numer. Anal.*, 28:149–167, 2008.
- [16] J. Chung and A. K. Saibaba. Generalized hybrid iterative methods for large-scale Bayesian inverse problems. *arXiv preprint arXiv:1607.03943*, 2016.
- [17] H. P. Flath, L. C. Wilcox, V. Akçelik, J. Hill, B. van Bloemen Waanders, and O. Ghattas. Fast algorithms for Bayesian uncertainty quantification in large-scale linear inverse problems based on low-rank partial Hessian approximations. *SIAM J. Sci. Comput.*, 33(1):407–432, 2011.
- [18] C. Fox. Recent advances in inferential solutions to inverse problems. *Inverse Probl. Sci. Eng.*, 16(6):797–810, 2008.
- [19] C. Fox and R. A. Norton. Fast sampling in a linear–Gaussian inverse problem. Arxiv Preprint 1507.01614, 2016.
- [20] D. Gamerman and H.F. Lopes. *Markov Chain Monte Carlo: Stochastic Simulation for Bayesian Inference*. Chapman & Hall/CRC, Boca Raton, 2006.
- [21] A. E. Gelfand and A. F. M. Smith. Sampling-based approaches to calculating marginal densities. *J. Amer. Statist. Assoc.*, 85(410):398–409, 1990.
- [22] A. Gelman. Prior distributions for variance parameters in hierarchical models. *Bayesian Anal.*, 1(3):515–533, 2006.
- [23] A. Gelman, J. B. Carlin, H. S. Stern, D. B. Dunson, A. Vehtari, and D. B. Rubin. *Bayesian Data Analysis*. Chapman & Hall/CRC, Boca Raton, 3rd edition, 2014.
- [24] A. Gelman, G. Roberts, and W. Gilks. Efficient Metropolis jumping rules. In J. M. Bernardo, J. O. Berger, A. P. Dawid, and A. F. M. Smith, editors, *Bayesian Statistics 5*, volume 5, pages 599–607. Oxford University Press, New York, 1995.
- [25] A. Gelman and D. B. Rubin. Inference from iterative simulation using multiple sequences (with discussion). *Statist. Sci.*, 7:457–511, 1992.
- [26] S. Geman and D. Geman. Stochastic relaxation, Gibbs distributions and the Bayesian restoration of images. *IEEE Transactions on Pattern Analysis and Machine Intelligence*, 6:721–741, 1984.
- [27] G. Gomez-Herrero. Simulating and estimating EEG sources. http://germangh.github.io/tutorials/dipoles/tutorial_dipoles.htm. Accessed: 2016-06-22.
- [28] P. C. Hansen. Analysis of discrete ill-posed problems by means of the L-curve. *SIAM Rev.*, 34(4):561–580, 1992.
- [29] P. C. Hansen. Regularization tools version 4.0 for Matlab 7.3. *Numer. Algorithms*, 46:189–194, 2007.
- [30] P. C. Hansen. *Discrete inverse problems: insight and algorithms*, volume 7. SIAM, 2010.

- [31] P. C. Hansen and D. P. O’Leary. The use of the L-curve in the regularization of discrete ill-posed problems. *SIAM J. Sci. Comput.*, 14(6):1487–1503, 1993.
- [32] O. Hauk. Keep it simple: A case for using classical minimum norm estimation in the analysis of EEG and MEG data. *NeuroImage*, 21:1612–1621, 2004.
- [33] D. Higdon, J. Gattiker, B. Williams, and M. Rightley. Computer model calibration using high-dimensional output. *J. Amer. Statist. Assoc.*, 103:570–583, 2008.
- [34] D. Higdon, H. Lee, and C. Holloman. Markov chain Monte Carlo-based approaches for inference in computationally intensive inverse problems. In J. M. Bernardo, M. J. Bayarri, J. O. Berger, A. P. Dawid, D. Heckerman, A. F. M. Smith, and M. West, editors, *Bayesian Statistics 7: Proceedings of the Seventh Valencia International Meeting*, pages 181–197. Oxford University Press, 2003.
- [35] A. E. Hoerl and R. W. Kennard. Ridge regression: Biased estimation for nonorthogonal problems. *Technometrics*, 12(1):55–67, 1970.
- [36] R. A. Johnson and D. W. Wichern. *Applied Multivariate Statistical Analysis*. Prentice Hall, Upper Saddle River, 6th edition, 2007.
- [37] J. Kaipio and E. Somersalo. *Statistical and Computational Inverse Problems*. Springer, New York, 2005.
- [38] R. E. Kass, B. P. Carlin, A. Gelman, and R. Neal. Markov chain Monte Carlo in practice: A roundtable discussion. *Amer. Statist.*, 52:93–100, 1998.
- [39] M. E. Kilmer and D. P. O’Leary. Choosing regularization parameters in iterative methods for ill-posed problems. *SIAM J. Matrix Anal. Appl.*, 22(4):1204–1221, 2001.
- [40] F. Lindgren, H. Rue, and J. Lindström. An explicit link between Gaussian fields and Gaussian Markov random fields: the stochastic partial differential equation approach. *J. R. Stat. Soc. Ser. B. Stat. Methodol.*, 73(4):423–498, 2011.
- [41] J. S. Liu, W. H. Wong, and A. Kong. Covariance structure of the Gibbs sampler with applications to the comparisons of estimators and augmentation schemes. *Biometrika*, 84:27–40, 1994.
- [42] J. Mead. Parameter estimation: A new approach to weighting a priori information. *J. Inverse Ill-Posed Probl.*, 16(2):175–194, 2008.
- [43] J. L. Mead and R. A. Renaut. A Newton root-finding algorithm for estimating the regularization parameter for solving ill-conditioned least squares problems. *Inverse Problems*, 25(2):025002, 2008.
- [44] K. Mosegaard and A. Tarantola. Probabilistic Approach to Inverse Problems. In *International Handbook of Earthquake & Engineering Seismology, Part A.*, pages 237–265. Academic Press, 2002.
- [45] P. Müller. A generic approach to posterior integration and Gibbs sampling. Technical Report, Purdue University, 1991.
- [46] C. Nahkhleh, D. Higdon, C. K. Allen, and R. Ryne. Bayesian reconstruction of particle beam phase space. In *Bayesian Theory and Applications*, pages 673–686. Oxford University Press, 2013.
- [47] R. M. Neal. Regression and classification using Gaussian process priors. In J. M. Bernardo, J. O. Berger, A. P. Dawid, and A. F. M. Smith, editors, *Bayesian Statistics 6*, volume 6, pages 475–501. Oxford University Press, New York, 1998.

- [48] M. D. Nunez, P. Nunez, and R. Srinivasan. Electroencephalography (EEG): Neurophysics, experimental methods, and signal processing. In H. Ombao, M. Lindquist, W. Thompson, and J. Aston, editors, *Handbook of Statistical Methods for Brain Signals and Images*, pages 175–197. Chapman & Hall/CRC, Boca Raton, 2016.
- [49] R. Oostenveld, P. Fries, E. Maris, and J.-M. Schoffelen. FieldTrip: Open source software for advanced analysis of MEG, EEG, and invasive electrophysiological data. *Comput. Intell. Neurosci.*, 2011:156869, 2011.
- [50] F. O’Sullivan. A Statistitcal Perspective on Ill-Posed Inverse Problems. *Statist. Sci.*, 1(4):502–527, 1986.
- [51] W. Penny, S. Kiebel, and K. J. Friston. Variational Bayesian inference for fMRI time series. *NeuroImage*, 19(3):727–741, 2003.
- [52] N. Petra, J. Martin, G. Stadler, and O. Ghattas. A computational framework for infinite-dimensional Bayesian inverse problems, part ii: stochastic Newton MCMC with application to ice sheet flow inverse problems. *SIAM J. Sci. Comput.*, 36(4):A1525–A1555, 2014.
- [53] N. G. Polson and J. G. Scott. Shrink globally, act locally: Sparse Bayesian regression and prediction. In J. M. Bernardo, M. J. Bayarri, J. O. Berger, A. P. Dawid, D. Heckerman, A. F. M. Smith, and M. West, editors, *Bayesian Statistics 9*, pages 501–538. Oxford University Press, 2010.
- [54] A.V. Prokhorov. Chebyshev inequality in probability theory. Encyclopedia of Mathematics. http://www.encyclopediaofmath.org/index.php?title=Chebyshev_inequality_in_probability_theory&oldid=26393.
- [55] C. E. Rasmussen and C. K. I. Williams. *Gaussian Processes for Machine Learning*. MIT Press, Cambridge, 2006.
- [56] S. I. Resnick. *Adventures in Stochastic Processes*. Birkhäuser, Boston, 1992.
- [57] C. Robert and G. Casella. *Monte Carlo Statistical Methods*. Springer, New York, 2nd edition, 2004.
- [58] J. S. Rosenthal. Optimal proposal distributions and adaptive MCMC. In S. Brooks, A. Gelman, G. L. Jones, and X.-L. Meng, editors, *Handbook of Markov Chain Monte Carlo*, pages 93–111. Chapman & Hall/CRC, Boca Raton, 2011.
- [59] H. Rue and L. Held. *Gaussian Markov Random Fields*. Chapman & Hall/CRC, Boca Raton, 2005.
- [60] Y. Saad. *Numerical methods for large eigenvalue problems*, volume 158. SIAM, 1992.
- [61] A. K. Saibaba and P. K. Kitanidis. Efficient methods for large-scale linear inversion using a geostatistical approach. *Water Resour. Res.*, 48(5), 2012.
- [62] A. K. Saibaba and P. K. Kitanidis. Fast computation of uncertainty quantification measures in the geostatistical approach to solve inverse problems. *Adv. Water Resour.*, 82(0):124–138, 2015.
- [63] T. J. Santner, B. J. Williams, and W. I. Notz. *The Design and Analysis of Computer Experiments*. Springer-Verlag, New York, 2003.
- [64] O. Scherzer. The use of Morozov’s discrepancy principle for Tikhonov regularization for solving nonlinear ill-posed problems. *Computing*, 51(1):45–60, 1993.
- [65] J. G. Scott and J. O. Berger. An exploration of aspects of Bayesian multiple testing. *J. Statist. Plann. Inference*, 136(7):2144–2162, 2006.

- [66] C. B. Shaw. Improvements of the resolution of an instrument by numerical solution of an integral equation. *J. Math. Anal. Appl.*, 37:83–112, 1972.
- [67] L. A. Shepp and B. F. Logan. The Fourier reconstruction of a head section. *IEEE Trans. Nucl. Sci.*, 21(3):21–43, 1974.
- [68] H. D. Simon and H. Zha. Low-rank matrix approximation using the Lanczos bidiagonalization process with applications. *SIAM J. Sci. Comput.*, 21(6):2257–2274, 2000.
- [69] Alessio Spantini, Antti Solonen, Tiangang Cui, James Martin, Luis Tenorio, and Youssef Marzouk. Optimal low-rank approximations of Bayesian linear inverse problems. *SIAM Journal on Scientific Computing*, 37(6):A2451–A2487, 2015.
- [70] A. M. Stuart. Inverse problems : A Bayesian perspective. *Acta Numer.*, 19(May):451–559, 2010.
- [71] G. C. Tiao and W. Tan. Bayesian analysis of random-effect models in the analysis of variance, I. Posterior distribution of variance components. *Biometrika*, 51:37–53, 1965.
- [72] L. Tierney. Markov chains for exploring posterior distributions. *Ann. Statist.*, 22(4):1701–1762, 1994.
- [73] A. N. Tikhonov and V. Y. Arsenin. *Solutions of Ill-Posed Problems*. Winston, Washington, D. C., 1977.
- [74] C. R. Vogel. *Computational Methods for Inverse Problems*. SIAM, 2002.
- [75] Y. Zhao, J. Kang, and Q. Long. Bayesian multiresolution variable selection for ultra-high dimensional neuroimaging data. *IEEE/ACM Trans. on Comp. Biol. and Bioinform.*, 2015. to appear.